1 **Revision 1**

2 Heavy halogen compositions of lamprophyres derived from 3 metasomatized lithospheric mantle beneath eastern North China 4 Craton

5 Word Count: 6309

6

7 Yixin Zheng[1], Zaicong Wang[1]*, Tao He[1], Ray Burgess[2], Zhaoxian Zhu[1], Lian-Xun Wang[1],
8 Xiang Wang[1], Zhaochu Hu[1], Yongsheng Liu[1]
9 [1] *State Key Laboratory of Geological Processes and Mineral Resources, and School of*
10 *Earth Sciences, China University of Geosciences, Wuhan 430074, China*
11 [2] *School of Earth and Environmental Science, The University of Manchester, Oxford Road,*
12 *Manchester M13 9PL, UK*
13 *Correspondence to Zaicong Wang, zaicongwang@cug.edu.cn

14

15 **ABSTRACT**

16 Halogens and other volatiles are widely recycled into the deep mantle by subduction
17 and are key components to metasomatize the sub-continental lithospheric mantle (SCLM).
18 Lamprophyres are well-known to be rich in volatiles and are important for understanding
19 the halogen characteristics of the metasomatized SCLM and/or the mobilization of

halogens during the ascent of such volatile-rich, low-degree partial melts. The North China Craton (NCC) hosts lamprophyre dikes coeval with extensive thinning of the eastern NCC in the Mesozoic and generated from lithosphere metasomatized by multiple-stage subduction components. Here we report bulk-rock heavy halogens (Cl, Br, and I) of 16 lamprophyres from the eastern NCC. The bulk-rock halogen concentrations are overall very low (Cl = 58–170 μg/g, Br = 285–559 ng/g, and I less than 5 ng/g), comparable with depleted Mid-Ocean ridge basalts (N-MORBs). Volatile-rich minerals (e.g., amphibole and biotite) are abundant (20–30 vol.%) in these lamprophyres, however, EPMA data indicate that amphiboles are mainly rich in OH and F but display very low Cl concentrations (0.01–0.04 wt.%). The bulk rock and amphibole data consistently indicate low abundances of heavy halogens in the lamprophyres, which is difficult to reconcile with the remarkable enrichment of fluid-mobile large ion lithophile elements such as Ba, Rb, and K. Based on low Cl/Nb and Br/Nb but high Ba/Nb and K/Nb ratios, the low halogen concentrations likely resulted from extensive volatile loss (> 90%) during melt ascent. The low Cl concentrations in early-stage amphiboles (Mg# 60–64) further indicate that such loss would have occurred before amphibole crystallization at a depth of approximately 15 km. We thus propose that crystallization of early olivines and pyroxenes and reaction with surrounding mantle rocks likely induced volatile saturation and exsolution, leading to strong partitioning of the halogens into the exsolved aqueous

volatile phases and thus the extensive loss of halogens from the rising melt. These results reveal that significant volatile loss of halogens not only occurs during surficial low-pressure eruption but also at much deeper levels in the crust, as also identified for some kimberlites. Consequently, it would be difficult to constrain the primitive halogen components of the mantle sources via lamprophyres or similar magmas.

Keywords: Halogen, Lamprophyres, Deep degassing, Metasomatized mantle, North China Craton

INTRODUCTION

Recycling of volatiles into the mantle at subduction zones has a profound impact on the geochemical evolution of the Earth's mantle (e.g., Barnes et al., 2018; Bekaert et al., 2021; Broadley et al., 2016; Kendrick et al., 2020; Wallace, 2005). The oceanic lithosphere (including the oceanic crust and lithospheric mantle) is rich in volatiles due to interaction with seawater and hydrothermal fluids (e.g., Kendrick et al., 2011; Pagé et al., 2016). The serpentinized lithospheric mantle is considered to be the main carrier of the deep halogen cycle (e.g., Kendrick et al., 2017; Kendrick et al., 2013; Pagé and Hattori, 2019). The subducted halogens play an important role in controlling the diffusion, viscosity, density, and phase equilibrium of silicate melts (e.g., Baasner et al., 2013; Feisel et al., 2022; Filiberto and Treiman, 2009a; Filiberto and Treiman, 2009b; Thomas and Wood, 2021; Zimova and Webb, 2006). On a mole by mole basis, chlorine has twice the effect of water on lowering the liquidus temperature of basalt (Filiberto and Treiman, 2009a). Chlorine is also an important ligand in hydrothermal fluids, influencing the migration and mineralization processes of economically important metals such as Cu and Au (Blundy et al., 2015; Zajacz et al., 2010). Furthermore, the release of halogens from the metasomatized lithospheric mantle to the terrestrial surface could affect the atmosphere and hydrosphere (von Glasow et al., 2009) and even destroy the ozone layer potentially contributing to mass extinctions (Broadley et al., 2018a).

Despite their geochemical and environmental importance, the halogen compositions of samples of metasomatized lithospheric mantle have been relatively poorly studied. Most studies of mantle halogens have focused on oceanic settings, including systematic measurement of Cl, Br, and I concentrations of mantle-derived melts such as mid-ocean ridge basalts (MORBs) and arc and back-arc lavas as well as mantle xenoliths (peridotites and pyroxenites) from subduction zones (e.g., Broadley et al., 2016; Kendrick et al., 2020; Kendrick et al., 2017; Kendrick et al., 2014b; Kobayashi et al., 2017; Saal et al., 2002; Sumino et al., 2010). The oceanic lithospheric mantle is considered to be an important halogen reservoir (Frezzotti and Ferrando, 2018). By contrast, the enrichment levels of halogens in the metasomatized sub-continental lithospheric mantle (SCLM) are less well-studied (e.g., Broadley et al., 2016; Broadley et al., 2018b; Burgess et al., 2002; Toyama et al., 2021). Available data are mainly from continental lithospheric mantle xenoliths and diamond inclusions but they show large variations in the halogen concentrations (e.g., Broadley et al., 2016; Broadley et al., 2018a; Burgess et al., 2002; Hecker et al., 2020; Kobayashi et al., 2019). Halogen behavior in melts and magmatic fluids remains an area of limited understanding. It is generally accepted that the release of halogens in magma occurs mainly at a shallow level (Harford, 2003; Lowenstern et al., 2012; Wang et al., 2014), but studies on kimberlites have found that continuous volatile exsolution also occurs in deep regions (Russell et al., 2012; Russell et al., 2019). Overall,

84 the halogen release processes during the magmatic migration remain unclear including
85 the release triggers, release depths, and quantities.

86 Lamprophyres are produced by preferential partial melting of metasomatized
87 portions of the SCLM (e.g., Dongre and Tappe, 2019; Maria and Luhr, 2008; Rock et al.,
88 1991; Wang et al., 2022). They are often rich in hydrous minerals (e.g., amphibole and
89 biotite), volatiles (e.g., S, Cl, and H_2O), alkalis, fluid-mobile incompatible elements (e.g.,
90 K, Ba, and Rb) (e.g., Rock, 1987; Rock and Groves, 1988; Wang et al., 2022). Since
91 lamprophyres are derived from relatively large regions of mantle then, in the absence of
92 significant crustal contamination and other secondary processes, they are more
93 homogeneous and representative than mantle xenoliths (Wang et al., 2022; Wang et al.,
94 2020), and could better reflect the nature of the SCLM from a broader domain, as well as
95 the mobilization of halogens during the ascent of lamprophyre melts.

96 The North China Craton (NCC) has been stable, with no extensive magmatic activity,
97 since its formation in the Archean (e.g., Wu et al., 2019). The Paleozoic kimberlites in
98 eastern NCC (e.g., Li et al., 2011) have relatively high halogen concentrations relative to
99 kimberlites from other cratons, implying that the SCLM beneath NCC is a potential
100 reservoir with high halogen concentrations (Toyama et al., 2021). During the Mesozoic,
101 the SCLM was strongly metasomatized and hydrated by subducted components (e.g., Liu
102 et al., 2019; Wang et al., 2020; Wu et al., 2019). Lamprophyre dikes derived from the

103 metasomatized lithospheric mantle are widely distributed in the Jiaodong Peninsula. (e.g.,
104 Ma et al., 2014b; Wang et al., 2020; Windley et al., 2010). In this regard, the halogen
105 compositions of lamprophyres in the eastern NCC can provide new insights into
106 metasomatized SCLM and halogen behavior during magma ascent. To address these
107 issues, here we have examined the bulk-rock compositions of heavy halogens (Cl, Br, and
108 I) and *in-situ* Cl concentrations in amphiboles of the lamprophyres originating from the
109 metasomatized mantle in Jiaodong Peninsula, eastern NCC.
110

111 ## GEOLOGICAL SETTING AND SAMPLE DESCRIPTION

112 ### Geological setting

113 The eastern NCC is one of the oldest Archean cratons in the world, with crustal rocks
114 as old as 3.8 Ga (e.g., Kusky et al., 2007; Zhao et al., 2001). It has remained relatively
115 stable since its cratonization in Archean-Paleoproterozoic until it was affected by mantle
116 metasomatism related to multi-stage subduction events in the Mesozoic (e.g., Wu et al.,
117 2019). In the Triassic, the Yangtze craton collided from south to north and subducted
118 beneath the NCC (e.g., Ernst et al., 2007). The NCC was further influenced by the
119 subduction of the Paleo-Pacific plate from the east in the Jurassic (e.g., Liu et al., 2019;
120 Wu et al., 2019; Zheng et al., 2018). Following these subduction events, the SCLM
121 beneath the eastern NCC was strongly modified and hydrated by subducted slab-derived

melts/fluids (e.g., Liu et al., 2019; Wang et al., 2020). Lithospheric thinning and extensive crustal extension occurred during the Late Mesozoic, which triggered partial melting of the metasomatized SCLM and extensive magmatism (e.g., Lin and Wei, 2018; Wu et al., 2019; Zheng et al., 2018). Lamprophyre dykes were widely present in the eastern NCC and were mainly formed between 130–120 Ma, consistent with the peak time of the NCC destruction (e.g., Dai et al., 2016; Guo et al., 2004; Shen et al., 2009; Wang et al., 2020). Previous studies proposed that these lamprophyres were derived from the metasomatized and enriched lithospheric mantle (e.g., Ma et al., 2014a; Ma et al., 2014b; Wang et al., 2022; Wang et al., 2020).

Sample description

Lamprophyre samples in this study were collected from different locations of the Jiaodong Peninsula, eastern NCC: Linglong, Zhaoyuan, and Qixia districts (Fig. 1). The lamprophyres collected in the underground tunnel of the Linglong gold mine (Fig. 2a; N=12) are far away from gold-bearing quartz veins, and there is no effect of hydrothermal alteration (Wang et al., 2020). Other lamprophyres were collected from the surface outcrop in Qixia (N=3) and Zhaoyuan (N=1) districts which were far from the gold mines (Wang et al., 2020). Chlorine is an important mineralizing agent for gold deposits and is dissolved in ore-forming fluids (Aiuppa et al., 2009; Zajacz et al., 2010). This sampling strategy avoided the effect of secondary overprint of ore-forming fluids, as

141 emphasized by Taylor et al. (1994) and Wang et al. (2022).

142 Lamprophyres are dark green to gray-black in hand specimens. Phenocrysts are
143 mainly composed of hydrous minerals such as amphibole and biotite, comprising up to
144 20–30 vol.%, as well as a small proportion of nominally-volatile-free minerals such as
145 olivine and clinopyroxene (Fig. 2b). The groundmass includes amphibole, plagioclase,
146 alkali feldspar, biotite, and minor carbonate (Fig. 2). The presence of euhedral olivine and
147 clinopyroxene as well as hydrous minerals indicate that they crystallized from primitive
148 and hydrous magmas. The high loss on ignition (LOI: 3.5–11.3 wt.%) mainly reflects the
149 primary volatile-rich feature of lamprophyres. Secondary alteration is mainly manifested
150 by partial replacement of olivine, clinopyroxene, and even plagioclase in the matrix and a
151 certain degree of chloritization has occurred (Figs. 2e and 2f). The alteration may be
152 related to the autometasomatism occurring in water-rich lamprophyres (H_2O 2–4 wt.%)
153 during the late-stage magmatic process (Liang et al., 2019; Rock et al., 1991; Wang et al.,
154 2020).

155 The lamprophyres of this study have been studied in detail including petrology,
156 major and trace elements, chalcophile elements (e.g., S), Sr-Nd isotopes, and ages (130–
157 120 Ma) (Wang et al., 2022; Wang et al., 2020). They are K-rich calc-alkaline and
158 alkaline lamprophyres (K_2O 1.8–3.9 wt. %). The high Mg# values (molar ratio of
159 Mg/(Mg+Fe) *100, up to 74) and transition element concentrations of Cr (262–753 μg/g)

160 and Ni (113–303 μg/g) indicate that the lamprophyres have primitive magma properties
161 (Wang et al., 2020). The studied samples all display island arc basalt-like trace element
162 patterns, which are depleted in high field strength elements (HFSEs) and enriched in
163 fluid-mobile large ion lithophile elements (LILEs) (Fig. 3). Combined with radiogenic
164 $^{87}Sr/^{86}Sr$ (0. 70922–0.71211) and $^{143}Nd/^{144}Nd$ (0.51167–0.51190) isotopic compositions
165 (Fig. 3), these lamprophyres were generated from strongly metasomatized portions of the
166 SCLM by slab-derived fluids during the Mesozoic (Ma et al., 2014a; Wang et al., 2020).

This is the peer-reviewed, final accepted version for American Mineralogist, published by the Mineralogical Society of America.
The published version is subject to change. Cite as Authors (Year) Title. American Mineralogist, in press.
DOI: https://doi.org/10.2138/am-2022-8693. http://www.minsocam.org/

METHODS

During preparation, the altered surfaces of lamprophyres were removed with a rock saw, and the cut surfaces were abraded with silica emery paper. Following this, samples were washed with ultrapure Milli-Q water of 18.2 MΩ cm^{-1} before being dried and processed into rock powder. All procedures avoided possible contamination of halogens during sample processing.

Bulk-rock halogen analysis

Bulk-rock halogen concentrations were determined by a rapid and efficient method developed for geological rock samples (He et al., 2019). This method uses ammonium hydrogen fluoride (NH_4HF_2) to digest rock powder at 230°C for 2 hours. The NH_4HF_2 reagent efficiently decomposes silicate samples and also avoids the possible volatile loss of halogens via the formation of ammonium halide during sample digestion (He et al., 2019). Aliquots of 10 μg L^{-1} Te were added to the sample supernatant solution as the internal standard. The samples were then measured by high-sensitivity sector field ICP-MS (Element XR) at low-resolution mode for Br and I, but medium-resolution mode for Cl at the State Key Laboratory of Geological Processes and Mineral Resources, China University of Geosciences, Wuhan (GPMR-CUG). The detection limits of Cl, Br, and I in rocks were 5 μg/g, 2 ng/g, and 5 ng/g, respectively.

An international basalt standard (USGS, BHVO-2) was processed together with

186 samples to monitor the quality of the digestion and analysis procedures. The Cl, Br, and I
187 results of BHVO-2 were 99 μg/g, 252 ng/g, and 42 ng/g, respectively, within the
188 previously reported range (81–104 μg/g for Cl, 240–295 ng/g for Br, and 16–307 ng/g for
189 I) (e.g., Agnès and Villemant, 2007; Balcone-Boissard et al., 2009; Kendrick et al., 2018;
190 Sekimoto and Ebihara, 2017; Wang et al., 2010). In our lab, multiple determinations of
191 iodine concentrations in BHVO-2 displayed constant results, indicating the reliability of
192 this method (He et al., 2019).

193 **Electron probe microanalyses (EPMA) of amphibole**

194 Major and trace element analyses of amphibole have been performed with a JEOL
195 JXA-8230 electron probe microanalyser equipped with a 5-channel spectrometer in the
196 Laboratory of Microscopy and Microanalysis of Wuhan Microbeam Detection
197 Technology Co., LTD. Prior to acquiring the element contents, optical and electron
198 microscopy images were obtained for each amphibole grain to assess the level of any
199 alteration and zonation and to assist in selecting EPMA positions (Fig. 2). Based on these
200 results, we selected four amphiboles from the fresh lamprophyre sample 17XS26 for
201 *in-situ* analyses.

202 A thin section was coated by carbon film with a uniform thickness of about 20 nm,
203 following the experimental method by Zhang and Yang (2016). The primary acceleration
204 voltage was 15 kV, and a 20 nA beam current and a 10 μm beam spot diameter were used

for all mineral analyses. The major element content, as well as F and Cl concentrations of amphiboles, were measured by EPMA. The analysis times of characteristic peaks of F, C1, Na, Mg, A1, Si, K, Ca, Fe, Ni, and Cr are 10 s, while Ti and Mn are 20 s. The standard samples used for testing elements were fluorite (F), sodium chloride (Cl), jadeite (Na), diopside (Mg, Ca), magnesium aluminite (Fe, A1), olivine (Si), potassium feldspar (K), rutile (Ti), rhodonite (Mn), nickel (Ni), and chromium oxide (Cr). The detection limits for F and Cl were ~330 μg/g and ~37 μg/g, respectively.

RESULTS

Halogen compositions

The 16 lamprophyre samples have similar halogen compositions (Table 1). The concentrations of Cl and Br are 58–170 μg/g, and 285–559 ng/g, respectively, and the I concentrations are all below the detection limit of 5 ng/g (Fig. 4). The halogen concentrations do not change systematically with magmatic evolution index (MgO) or other major and trace elements (Figs. 4, 5, 6a and 6b). As Fig 4 shows, the halogen compositions of lamprophyres are close to those of N-MORBs (14–225 μg/g Cl, 35–34 ng/g Br), which are generally lower than that of E-MORBs (Cl mean of 371 μg/g, Br mean of 1123 ng/g), and arc-related lavas (Cl mean of 972 μg/g, Br mean of 2825 ng/g) (calculated from Kendrick et al., 2020; Kendrick et al., 2017).

Eight samples in this study have Br/Cl ratios of 0.002–0.004, which are within the range of MORBs and OIBs (0.0028 ± 0.0008) (Kendrick et al., 2017). However, the other eight samples have notably higher Br/Cl ratios of about 0.007–0.008 (Table 1).

Mineral chemistry

We performed electron probe microanalyses (N=27) on four amphiboles from the fresh lamprophyre 17XS26 (Table 2). The magmatic amphiboles have similar Mg# ranging from 64 to 66. They display a magnesiohastingsite composition characterized by TiO_2 and CaO contents ranging from 2.4 to 3.0 wt.% and from 11.3 to 11.5 wt.% respectively (Leake and Elgey, 1997). The Cl concentrations of amphiboles are similarly low, ranging between 0.01 and 0.04 wt.% with an average value of 0.02 wt.%. Physiochemical parameters (P, T, H_2O_{melt}) at the time of amphibole crystallization were estimated using the empirical formulations provided by Ridolfi and Renzulli (2012) based on amphibole composition. These amphiboles record similar pressure, temperature, and melt water content estimates of 340–420 MPa, 907–925°C, and 6.18 ± 0.1 wt.%, respectively. The corresponding crystallization depth is 12.8–15.9 km with an average of 14.2 km (Table 2). The details are presented in Table S2. Based on the EPMA data of clinopyroxenes provided by Wang et al. (2020), the crystallization temperature and pressure of clinopyroxenes were further estimated using the method proposed by Putirka (2008). The crystallization depth of clinopyroxene is about 20 km, except for one sample

(17QX20C, 10.5 km). The crystallization temperature of clinopyroxene is about 1200 ℃. The Mg# is about 84 on average, which is higher than amphibole indicating the earlier crystallization (Table S3).

DISCUSSION

Heavy halogens in the lithospheric mantle beneath the NCC

The incompatible behavior of volatiles during magmatic processes leads to their depletion from the mantle and the enrichment in the crust (e.g., Hilton et al., 2002). Whether volatiles can be recycled back into the mantle through subduction zones has been widely discussed (e.g., Barnes et al., 2018a; Kendrick et al., 2020; Schilling et al., 1978; Wallace, 2005). Numerous studies have shown that the subducted volatiles are effectively released in the forearc or sub-arc region during subduction (Dixon et al., 2002; Ito et al., 1983; Schilling et al., 1978; Wallace, 2005). Mass balance calculations indicate that the predominant fraction of slab-derived Cl is returned to the Earth's surface (e.g., Barnes et al., 2018; Ito et al., 1983; Ruscitto et al., 2012). However, up to 10% of the total subducted Cl may survive into the deep mantle (e.g., Kendrick et al., 2014a; Kendrick et al., 2020). Similarly, Br and I can also be added to the mantle (e.g., Barnes et al., 2018; Pyle and Mather, 2009). Deep Cl recycling is also evidenced by Br/Cl, I/Cl, and Cl/K ratios and chlorine isotope compositions of plume-related basalts (e.g., John et al.,

2010; Kendrick et al., 2014b; Stroncik and Haase, 2004; Workman et al., 2006). It has also been reported that the diamonds from the deep mantle captured slab-derived highly saline fluid inclusions (Johnson et al., 2000; Tomlinson et al., 2006; Weiss et al., 2015). It is further suggested that the SCLM beneath the continental subduction zone is rich in halogens because of the continuous addition of halogens from the subducted plate (e.g., Broadley et al., 2016; Broadley et al., 2018a). These results convincingly indicate that subducted halogens can be recycled into the mantle and enriched at the base of the SCLM.

Paleozoic kimberlites in the NCC at Shandong (Jining and Mengyin) and Liaoning (Wafangdian) regions () were emplaced at approximately 480 Ma (Fig. 1a; Li et al., 2011). Although their isotopic features suggested different magma sources (Fig. 3), all of them show noticeably high halogen concentrations (Figs. 4c and 4d). The concentrations of Cl, Br, and I of these kimberlites are 640–2150 μg/g, 4.6–30.1 μg/g, and 0.028–0.083 μg/g, respectively (Table S4); higher by an order of magnitude than kimberlites from South Africa, Greenland, and Brazil, while the degree of incipient melting in the kimberlite source region would not be significantly different (Toyama et al., 2021). The results from kimberlites indicate high abundances of halogens stored in the lithospheric mantle beneath the NCC in the Paleozoic (Toyama et al., 2021). The lithospheric mantle was further strongly metasomatized and hydrated by aqueous melts and/or fluids from the

281 subducted continental and oceanic plates during the Mesozoic (see Geological Setting
282 section). Clinopyroxenes in Feixian basalts which erupted in the early Cretaceous (~120
283 Ma) (Fig. 1a), suggest high H_2O contents of > 1000 μg/g for the metasomatized SCLM of
284 the eastern NCC (Xia et al., 2019; Xia et al., 2013). Such values are dramatically higher
285 than the MORB source region (50–200 μg/g H_2O) and suggest abundant water and other
286 volatiles retained at the base of the NCC's lithospheric mantle, possibly added during
287 multi-stage subduction of oceanic plates since the Paleozoic (Xia et al., 2013). It is
288 suggested that some fluids released by dehydration of subducted plates during subduction
289 are highly saline (Kent et al., 2002; Manning and Frezzotti, 2020). The Cl/H_2O ratios
290 preserved in undegassed melt inclusions from primitive arc basalts imply fluid salinities
291 typically ranging between 5 and 15 wt.% NaCl (Métrich and Wallace, 2008), consistent
292 with fluid inclusion data from high-pressure metamorphic rocks and mantle xenoliths
293 from subduction zones (Frezzotti and Ferrando, 2015; Kawamoto et al., 2013). The
294 generally high salinity of subduction-zone fluids provides favorable evidence for the
295 addition of large amounts of Cl (and presumably Br and I) to the SCLM together with the
296 water. In conclusion, the high halogens in the kimberlites from the NCC and intense
297 mantle metasomatism and hydration very likely indicate that the lithospheric mantle
298 beneath the NCC is a potential reservoir with high halogen concentrations.
299

This is the peer-reviewed, final accepted version for American Mineralogist, published by the Mineralogical Society of America.
The published version is subject to change. Cite as Authors (Year) Title. American Mineralogist, in press.
DOI: https://doi.org/10.2138/am-2022-8693. http://www.minsocam.org/

Strong depletion of heavy halogens in lamprophyres

The lamprophyres in this study were formed coevally with the Feixian basalts. Importantly, they also were derived from the SCLM of the eastern NCC which was strongly metasomatized by aqueous fluid and share similar island arc-like trace element patterns (strong enrichment of fluid-mobile LILEs such as K, Rb, and Ba) and radiogenic Sr-Nd isotopes (Fig. 3 and Table S1). Based on the model proposed by Rustioni et al. (2021), we estimate saline fluids with at least 7 wt.% NaCl are required to be released from the basaltic slab to the zone of melting in order to reproduce the trace element enrichment pattern of lamprophyres in this study, since the fluid/eclogite partition coefficients of the LILEs increase with salinity (Rustioni et al., 2021). Olivine-hosted glass inclusions in lamprophyres in Mexico showed high Cl concentrations of 0.15–0.28 wt.% (Fig. 4a), suggesting high halogen abundance in primitive magmas of lamprophyres (Maria and Luhr, 2008). However, the halogen compositions of lamprophyres in this study are similar to those of N-MORBs and generally much lower than arc-related lavas which have also experienced subduction-related metasomatism in their source regions (Fig. 4). The results indicate that heavy halogen concentrations in the lamprophyres are relatively low. Chlorine, Br, I, and Nb are similarly incompatible during partial melting (Kendrick et al., 2017). Therefore, positive correlations exist among Cl, Br, I, and Nb of MORBs and OIBs (Fig. 5). The enrichment of Cl, Br, and I relative to Nb in arc-related lavas reflects the addition of subduction components which are rich in fluid-mobile

320 halogens but depleted in fluid-immobile Nb (Kendrick et al., 2020). However, the Cl, Br,
321 and I concentrations in lamprophyres are similar to MORB at given Nb concentrations
322 (Fig. 5).

323 Due to the similar incompatibility of Cl, Br, I, and K, they are not easily fractionated
324 by mantle melting processes, thus in the absence of shallow-level assimilation (involving
325 contamination by seawater, altered oceanic crust, or brines), the ratios of these elements
326 in mantle-derived melts can represent the mantle source (Kendrick et al., 2017). The Cl/K
327 ratios of MORB and OIB which are free from seawater assimilation are within a small
328 range (0.02–0.14) with a median of 0.06 ± 0.01 (Kendrick et al., 2017) (Fig. 6c). The
329 relative abundances of Cl, Br, and K are also used as important tracers for
330 subduction-related processes (e.g., Kendrick et al., 2017; Stroncik and Haase, 2004). The
331 Cl/K ratios of arc and back-arc glasses (0.05–0.54) are slightly higher than those of
332 MORB and OIB, indicating fluid-related enrichment of Cl in subduction-zone magmas
333 which can be attributed to the addition of a Cl-rich component in subduction zones
334 (Kendrick et al., 2020; Pyle and Mather, 2009) (Fig. 6c). However, the Cl/K ratios of
335 lamprophyres are one order of magnitude lower than those of MORB and OIB, as well as
336 Br/K and I/K ratios (Fig. 6c, d and Fig. S1b). Such strong depletion can also be identified
337 from the ratios of halogens and fluid-mobile elements (e.g., K and Ba) to fluid-immobile
338 elements with similar incompatibility (e.g., Nb). Cl-Br-K-Ba elements exhibit similar

339 mobility during subduction processes and can be effectively added to the source regions
340 of arc magma, resulting in the enrichment of these elements in island arc samples (e.g.,
341 Barnes et al., 2018; Kendrick et al., 2020). For arc-related lavas, with progressive
342 metasomatism, the ratios of Cl/Nb, Br/Nb, K/Nb, and Ba/Nb are elevated relative to
343 MORBs (Fig. 7). The good correlations between lithophile elements (Ba/Nb and K/Nb)
344 and volatile elements (Cl/Nb and Br/Nb) (Fig. 7) also indicate negligible halogen-loss
345 during submarine eruption. However, the Cl/Nb and Br/Nb of lamprophyres remain low
346 at the MORB level, although they display high K/Nb and Ba/Nb ratios (Fig. 7). In
347 addition to lamprophyres with relatively low Cl, Br, and I abundances and low
348 halogen/Nb ratios, halogens are also decoupled from K and Ba (Fig. 7 and Fig. S1). Since
349 K, Ba, K/Nb, and Ba/Nb values do not vary so much for lamprophyres with different
350 degrees of alteration (see Alternation section), we exclude the possibility that these values
351 were increased by secondary alteration and advocate that elevated K/Nb and Ba/Nb
352 reflecting the original characteristics of lamprophyres. Overall, the results indicate strong
353 depletion of heavy halogens in lamprophyres.

354 The Cl concentrations of amphiboles in basaltic magma can reach several thousand
355 μg/g and even 1 wt.% (Webster et al., 2018), given relatively high amphibole/melt
356 partition coefficients for Cl in the hydrous basaltic melts (Dalou et al., 2014). Chlorine
357 concentrations for amphiboles in Andean basaltic-andesite volcanic rocks range from

358 0.15 wt.% to 0.24 wt.% (Chambefort et al., 2013; Webster et al., 2018); extremely
359 high-Cl amphiboles (3–5 wt.% Cl) were also found in mafic intrusion rocks of the
360 Kusa-Kopan complex (Shagalov et al., 2021). However, EPMA data of the amphiboles in
361 the lamprophyre in this study indicate very low Cl concentrations of 0.01–0.04 wt.%
362 (Table 2) which are consistent with amphiboles of calc-alkaline lamprophyres in Western
363 Australia (≤ 0.03 wt.%) (Choi et al., 2019). Consequently, the low halogens abundances
364 present in both amphibole and bulk-rock support the strong depletion of halogens in the
365 lamprophyres.

366 There is a good correlation between Cl, Br, I, and K of MORBs and some arc lavas
367 (Fig. 6a, b, and Fig. S1a), the latter being variably higher than that of MORBs. Using the
368 median values of Cl/K (0.091), Br/K (2.5×10^{-4}), and I/K (5.3×10^{-6}) of MORB and
369 measured K contents of lamprophyres (1.47–3.21 wt.%) in this study, the estimated
370 halogen concentrations of primary lamprophyre melts are 1332–2907 μg/g Cl, 3673–
371 8019 ng/g Br, and 78–170 ng/g I, respectively. The calculations indicate that
372 lamprophyres in this study have lost > 90% Cl, Br, and I (Table 1). Below we will discuss
373 the possible reasons for the strong depletion of heavy halogens in these lamprophyres.
374

375 **Possible causes for heavy halogen depletions in lamprophyres**

376 **Negligible effect of crustal contamination and secondary alteration.** Previous

377 studies have shown that crustal contamination has minimal effect on the Jiaodong mafic
378 dike magmas during their rapid ascent along the trans-lithospheric fault (Deng et al.,
379 2017; Liang et al., 2018). Limited crustal contamination of the studied lamprophyres is
380 indicated by constant $^{87}Sr/^{86}Sr$ and ε Nd(t) with increasing SiO_2 (Wang et al., 2020).
381 However, the lamprophyre dikes contain some inherited zircons (Wang et al., 2020),
382 raising the possibility of crustal-derived halogens being incorporated during melt
383 emplacement. Zircon U-Pb geochronology shows that the inherited zircons were mainly
384 incorporated from surrounding granites and Archean basement rocks of the Jiaobei
385 terrane which are mainly composed of tonalite-trondhjemite-granodiorite (TTG) gneisses,
386 amphibolites, and mafic granulites (Wang et al., 2020). If the strong depletion of halogens
387 in lamprophyres (>90%) is caused by crustal contamination, then it can only be
388 accounted for by a dilution effect of adding a large volume of low-halogen crustal
389 components.

390 However, Cl concentrations in granitoid rocks, amphibolites, and gneisses are overall
391 high, ranging from 50-1000 μg/g (e.g., Gao et al., 1998; Hanley and Koga, 2018; Teiber
392 et al., 2014; Tripathi et al., 2021). The halogen compositions of the bulk continental crust
393 are 244 μg/g for Cl, 0.88 μg/g for Br, and 0.71 μg/g for I (Rudnick and Gao, 2003). The
394 Cl/Nb and Br/Nb ratios of the bulk continental crust (31 and 0.11, respectively) are also
395 higher than those of the lamprophyre samples of this study (mean 17 and 0.06,

396 respectively). Thus, crustal contamination would have the opposite effect of increasing
397 the halogen concentrations and ratios (Cl/Nb and Br/Nb) of lamprophyres. Therefore,
398 crustal contamination is excluded as a process to account for the halogen abundances of
399 lamprophyres.

400 Although the lamprophyres chosen in this study are very fresh in hand specimen,
401 variable degrees of alteration are still observed at the microscopic scale, mainly
402 manifested as chloritization of mafic minerals (Fig. 2). According to the degree of
403 chloritization observed under the microscope, we arbitrarily divided the samples into
404 three sub-types for comparison: fresh, with negligible chloritization (17QX20B,
405 17QX20C, 17XS26); those with intense chloritization (17QX21, 17ZY26, 17XS16); and
406 the rest as slight chloritization. K, Ba, K/Nb, and Ba/Nb values are relatively consistent
407 for lamprophyres with different degrees of alteration. Nevertheless, as shown in Fig. 8a,
408 secondary low-temperature alteration tends to decrease Cl concentrations but slightly
409 increase Br concentrations. The alteration explains the higher Br/Cl ratios of altered
410 lamprophyres which is unrelated to melt evolution (Fig. 8b) and mantle metasomatism
411 (Fig. 8c). Since crustal contamination cannot be completely ruled out, it is also possible
412 that the addition of very small amounts of high Br/Cl crustal components could result in
413 high Br/Cl ratios in some lamprophyres. However, strong chloritization does not change
414 the halogen concentrations of lamprophyres by more than a factor of 3. Importantly, the

415 least altered lamprophyres still show low contents of heavy halogens (Table 1). Moreover,
416 the amphiboles in fresh, high Mg# lamprophyres also contain low Cl concentrations
417 (Table 2). Therefore, chloritization is not the main factor causing the depletion of
418 halogens of lamprophyres.

419 **Negligible effect of surficial degassing.** Due to the strong volatility and fluid
420 mobility of Cl and Br, degassing of the magma could be an important mechanism for
421 halogen depletion (e.g., Bureau et al., 2000; Spilliaert et al., 2006; Webster et al., 1999).
422 Magma degassing involves the partitioning of volatiles into the gas phases and exsolution
423 into the aqueous phases (Aiuppa et al., 2009). Partitioning halogens into the gas phase
424 mainly depends on the pressure of magma eruption. Typically, Cl and Br do not tend to
425 partition into the gas phase under high-pressure conditions (Aiuppa et al., 2009; Cadoux
426 et al., 2018). For instance, a significant loss of halogens does not occur in submarine
427 eruptions. Unni and Schilling (1978) proposed that Cl-loss by volcanic degassing only
428 becomes important for samples that erupted under less than ~500 m water depth. The
429 consistency of Cl concentrations in glass and melt inclusions of Tonga arc rear lavas
430 (dredged below water depths of 1300 to 1900 m) indicates the negligible effect of
431 halogen degassing during the submarine eruption (Park et al., 2015). Under continental
432 crust conditions, experiments show that the CO_2 vapor phase begins to release from
433 kimberlite melts at shallow depths of < 3 km in the upper crust (Hoare et al., 2021;

434 Moussallam et al., 2015).

435 The emplacement and crystallization pressure of the Jiaodong Peninsula granites (the
436 host rocks of lamprophyres) is about 400 MPa (depth > 10 km), which may represent the
437 minimum depth of lamprophyre emplacement (e.g., Dou et al., 2018; Wang et al., 2022).
438 The crystallization depth of amphibole may represent the emplacement depth of mafic
439 magmas. Due to the relatively deep crystallization depth of amphibole (depth ~ 15 km)
440 (Table 2) and high confining pressure, it is unlikely that there was sufficient surficial
441 degassing to account for the halogen loss from lamprophyres. In addition, sulfur is often
442 considered to be more volatile than Cl (Lesne et al., 2011; Webster et al., 2018), but most
443 of the lamprophyres did not experience significant sulfur degassing (Wang et al., 2022).
444 Therefore, the less volatile heavy halogens of deep emplaced lamprophyres are unlikely
445 to have been lost from the melts into the gas phase in large quantities. Combined with the
446 characteristics of early crystallized but Cl-poor amphiboles (Table 2), we conclude that a
447 large amount of halogen loss must have occurred at a relatively deep level, and prior to
448 amphibole crystallization.

449 **Deep volatile exsolution of lamprophyre magmas.** The intense metasomatism by
450 aqueous fluid led to volatile-bearing minerals, including amphiboles and minor
451 phlogopites, being formed in the lamprophyre source region (Fig. 9a) (Wang et al., 2020),
452 and are the main halogen carriers in the SCLM (Frezzotti and Ferrando, 2018). As

453 low-degree partial melting products from an amphibole-bearing peridotite source,
454 lamprophyres should have elevated halogen concentrations. However, our results indicate
455 lamprophyres of this study are strongly depleted in halogens (see Section 5.1). As
456 discussed above, secondary alteration and surficial degassing processes are unable to
457 account for the observed low halogen concentrations. Due to their overall high
458 electronegativity and propensity to form hydrogen halides, Cl and Br have high solubility
459 in aqueous fluids and readily exsolve from volatile-saturated melts during magmatic
460 degassing (e.g., Teiber et al., 2014; Webster et al., 2018). Therefore, we propose that
461 volatile exsolution at depth is the most plausible cause for the significant halogen
462 depletion in lamprophyres. The process is described below and shown schematically in
463 Fig. 9.

464 This mechanism should not be related to first boiling (degassing caused by
465 decompression; e.g., Webster et al., 1999) since the solubility of exsolved
466 chlorine-containing liquids is less affected by pressure (Webster and De Vivo, 2002). The
467 primary lamprophyre magmas are rich in water and other volatiles, as reflected by
468 abundant amphibole and biotite and high-water contents in amphibole (Fig. 2 and Table
469 2). During the ascent of lamprophyre magma, the continuous interaction with
470 surrounding mantle rocks causes SiO_2-enrichment of the melt which in turn decreases
471 volatile solubility, as observed in volatile-rich kimberlites (Russell et al., 2012; Russell et

al., 2019). The crystallization of nominally-volatile-free minerals (olivine, pyroxene, plagioclase, etc.) in silicate melts could increase the total volatile concentration and volatile activities of the residual melts (De Vivo et al., 2005; Webster, 2004). The crystallization of these minerals also results in the decreasing abundances of Ca, Mg, and Fe in the residual melt induced which further reduces the solubility of Cl dramatically (Webster and De Vivo, 2002). These chemical-driven processes are distinguished from physical changes (i.e., decompression) which would lead to the volatiles reaching saturation and exsolving from the melts into aqueous phases even under relatively high-pressure conditions.

Water is the most abundant volatile component in silicate melts, and the volatile exsolution process is largely controlled by aqueous fluid. The water content (~ 6 wt.%) of lamprophyre melt during amphibole crystallization is close to the water saturation curve of basaltic melt (Table 2 and Fig. S2). Therefore, it is possible that the samples in our study had reached fluid saturation and exsolved saline fluid before amphibole crystallization (Fig. S2).

Present studies show that the partitioning of Cl and Br between aqueous fluid and melt is mainly influenced by the melt composition (Cadoux et al., 2018). Waelkens et al. (2021) found that fluid-melt partition coefficients for Cl and Br are 30 and 41, respectively, and fluid exsolution is responsible for most of the halogen release in a

491 rhyolitic super-volcanic system. Values of $D_{Cl}^{f/m}$ and $D_{Br}^{f/m}$ for mafic melts are usually
492 lower than those for intermediate (andesitic and phonolitic) and silicic melts, however, it
493 is observed that $D_{Cl}^{f/m}$ ranges between 8 and 34 in a trachybasaltic melt system (Cadoux
494 et al., 2018 and references therein). The elevated $D_{Cl}^{f/m}$ is also strongly affected by the
495 higher Cl concentration in the melt (Cadoux et al., 2018; Webster et al., 1999).
496 Experiments for the basalt suggest $D_{Br}^{f/m}$ is about 5.0 at 1200 °C-100 MPa (Cadoux et al.,
497 2018). Based on experimental data, Bureau et al. (2000) suggested for albite melt at 200
498 MPa and 900°C the partition coefficients ($D^{f/m}$) of Cl, Br, and I are 8.1±0.2, 17.5±0.6,
499 and 104±7, respectively. We can conclude that due to the relatively high $D_{Cl}^{f/m}$, $D_{Br}^{f/m}$,
500 and $D_{I}^{f/m}$ for mafic melts, heavy halogens strongly partition into the exsolved aqueous
501 volatile phases and eventually separate from the melts which result in the loss of most
502 halogens (Fig. 9b). On the basis of our estimated theoretical values (Table 1) (i.e., the
503 halogen concentrations of the primitive melts) and the halogen concentrations of
504 lamprophyres (Table 1) (i.e., the halogen concentrations of the residual melt), we
505 calculated the apparent partition coefficients of three fresh ones which were 11–13, 8–9
506 and 15–17 for $D_{Cl}^{f/m}$, $D_{Br}^{f/m}$ and $D_{I}^{f/m}$, respectively. These values are consistent with
507 experimental ranges supporting the possibility of fluid exsolution as a mean to deplete
508 heavy halogens from lamprophyre melts. However, the volatile exsolution did not
509 significantly affect sulfur which was mainly retained in the melts as sulfide (Wang et al.,

510 2022). The Cl ion in the exsolved saline fluid would bond to metal or metalloid cations
511 such as K, Na, and Ba, taking away part of these elements from primary melts. However,
512 fluid exsolution may not necessarily reduce the abundances of these metal cations at
513 similar levels to halogens, as is widely observed in brine fluids exsolved from
514 magmatic-hydrothermal systems (Pokrovski et al., 2013). For example, the fluid/melt
515 partition coefficients for alkali metals (e.g., $D_K^{f/m} < 0.5$) are much lower than those for Cl,
516 which implies that these cations would not necessarily partition into fluid phases
517 (Pokrovski et al., 2013; Zajacz et al., 2008).

518 Given the presence of Cl-poor amphibole, we speculate that the fluid exsolution of
519 lamprophyres would have occurred at a depth of more than 15 km prior to amphibole
520 crystallization. Interestingly, this is close to the minimum depth range of fluid exsolution
521 (20–25 km) observed in volcanic systems (e.g., Longpré et al., 2017; Maria and Luhr,
522 2008; Roberge et al., 2007; Ubide et al., 2022). The F and Cl concentrations of
523 volatile-bearing minerals in plutonic systems are similar to those in volcanic systems
524 (Zhang et al., 2012). These results imply that the evolution of Cl in melts at depth
525 (plutonic systems) is similar to that observed in volcanic systems during magma ascent
526 and degassing.

IMPLICATIONS

Lamprophyre dikes were widely emplaced at 130–120 Ma in the Jiaodong Peninsula, eastern NCC, and they were derived from lithospheric mantle strongly metasomatized by subduction components. Given the relatively high halogen abundances of kimberlites emplaced in the eastern NCC during the Paleozoic and the strong enrichment of fluid-mobile trace elements of lamprophyres, the mantle sources of these lamprophyres should have been rich in heavy halogens (Cl, Br, and I). However, the lamprophyres display very low abundances of heavy halogens. Based on the depletion of Cl/Nb and Br/Nb ratios relative to Ba/Nb and K/Nb, the heavy halogens likely underwent a significant loss of > 90% during the ascent of lamprophyre magmas. The amphiboles crystallized from high Mg# lamprophyres were poor in Cl but rich in water, suggesting that the halogen loss would have occurred before amphibole crystallization at crustal depths of > 15 km rather than during surficial degassing at low-pressure conditions. We propose that the volatile-rich primitive lamprophyre melts likely experienced volatile saturation and exsolution (partitioning into the exsolved aqueous volatile phases), resulting in a significant loss of heavy halogens.

Previous studies have suggested that shallow processes such as surface or near-surface crystallization or degassing often lead to intense loss of halogens (e.g., Lowenstern et al., 2012; Wang et al., 2014). Our present work on hydrous lamprophyres

546 further reveals that a large amount of halogen loss occurs during magma ascent at deep
547 crustal depth. Consequently, volatile-rich magmatic products such as lamprophyres
548 probably do not retain a record of the primary halogen characteristics of the source region,
549 and the Br/Cl ratios of the lamprophyres will not necessarily represent the SCLM source.
550 This study also implies the possibility that the lithospheric mantle of the eastern NCC
551 might represent an important halogen reservoir. Future studies combined with peridotite
552 xenoliths in eastern NCC may help illuminate the nature of this reservoir.
553

554 **ACKNOWLEDGEMENTS AND FUNDING**

555 The study was financially supported by the National Natural Science Foundation of
556 China (42273023, 41722302) and Chinese National Key Research and Development
557 Program (2016YFC0600103). We thank Jinhao Zheng and Haihong Chen for their
558 support in the laboratory and Zhe Xu and Zongqi Zou for their kind suggestions when
559 writing the first draft. We also appreciate two reviewers for their detailed and constructive
560 comments and Justin Filiberto for his editorial handling.

References

Agnès, M., and Villemant, B. (2007) Determination of Halogens (F, Cl, Br, I), Sulfur and Water in Seventeen Geological Reference Materials. Geostandards Newsletter, 27, 163-171.

Aiuppa, A., Baker, D.R., and Webster, J.D. (2009) Halogens in volcanic systems. Chemical Geology, 263(1-4), 1-18.

Baasner, A., Schmidt, B.C., and Webb, S.L. (2013) The effect of chlorine, fluorine and water on the viscosity of aluminosilicate melts. Chemical Geology, 357, 134-149.

Balcone-Boissard, H., Agnès, M., and Villemant, B. (2009) Simultaneous Determination of Fluorine, Chlorine, Bromine and Iodine in Six Geochemical Reference Materials Using Pyrohydrolysis, Ion Chromatography and Inductively Coupled Plasma - Mass Spectrometry. Geostandards and Geoanalytical Research, 33, 477-485.

Barnes, J.D., Manning, C.E., Scambelluri, M., and Selverstone, J. (2018) The Behavior of Halogens During Subduction-Zone Processes. In D.E. Harlov, and L. Aranovich, Eds. The Role of Halogens in Terrestrial and Extraterrestrial Geochemical Processes: Surface, Crust, and Mantle, p. 545-590. Springer International Publishing.

Bekaert, D.V., Turner, S.J., Broadley, M.W., Barnes, J.D., Halldórsson, S.A., Labidi, J., Wade, J., Walowski, K.J., and Barry, P.H. (2021) Subduction-Driven Volatile Recycling: A Global Mass Balance. Annual Review of Earth and Planetary Sciences, 49(1), 37-70.

Blundy, J., Mavrogenes, J., Tattitch, B., Sparks, S., and Gilmer, A. (2015) Generation of porphyry copper deposits by gas–brine reaction in volcanic arcs. Nature Geoscience, 8(3), 235-240.

Broadley, M.W., Ballentine, C.J., Chavrit, D., Dallai, L., and Burgess, R. (2016) Sedimentary halogens and noble gases within Western Antarctic xenoliths: Implications of extensive volatile recycling to the sub continental lithospheric mantle. Geochimica et Cosmochimica Acta, 176(8), 139-156.

Broadley, M.W., Barry, P.H., Ballentine, C.J., Taylor, L.A., and Burgess, R. (2018a) End-Permian extinction amplified by plume-induced release of recycled

592 lithospheric volatiles. Nature Geoscience, 11(9), 682-687.

593 Broadley, M.W., Kagi, H., Burgess, R., Zedgenizov, D., Mikhail, S., Almayrac, M.,
594 Ragozin, A., Pomazansky, B., and Sumino, H. (2018b) Plume-lithosphere
595 interaction, and the formation of fibrous diamonds. Geochemical Perspectives
596 Letters, 8, 26-30.

597 Bureau, H., Keppler, H., and Metrich, N. (2000) Volcanic degassing of bromine and
598 iodine: Experimental fluid/melt partitioning data and applications to stratospheric
599 chemistry. Earth and Planetary Science Letters, 183(1-2), 51-60.

600 Burgess, R., Layzelle, E., Turner, G., and Harris, J.W. (2002) Constraints on the age and
601 halogen composition of mantle fluids in Siberian coated diamonds. Earth and
602 Planetary Science Letters, 197(3-4), 193-203.

603 Cadoux, A., Iacono-Marziano, G., Scaillet, B., Aiuppa, A., Mather, T.A., Pyle, D.M.,
604 Deloule, E., Gennaro, E., and Paonita, A. (2018) The role of melt composition on
605 aqueous fluid vs. silicate melt partitioning of bromine in magmas. Earth and
606 Planetary Science Letters, 498(40), 450-463.

607 Chambefort, I., Dilles, J.H., and Longo, A.A. (2013) Amphibole geochemistry of the
608 Yanacocha Volcanics, Peru: Evidence for diverse sources of magmatic volatiles
609 related to gold ores. Journal of Petrology, 54(5), 1017-1046.

610 Choi, E., Fiorentini, M., Giuliani, A., Foley, S., Maas, R., and Taylor, W. (2019)
611 Subduction-related petrogenesis of Late Archean calc-alkaline lamprophyres in
612 the Yilgarn Craton (Western Australia). Precambrian Research, 338(105550),
613 1-17.

614 Dai, L.Q., Zheng, Y.F., and Zhao, Z.F. (2016) Termination time of peak decratonization in
615 North China: Geochemical evidence from mafic igneous rocks. Lithos, 240,
616 327-336.

617 Dalou, C., Koga, K.T., Le Voyer, M., and Shimizu, N. (2014) Contrasting partition
618 behavior of F and Cl during hydrous mantle melting: implications for Cl/F
619 signature in arc magmas. Progress in Earth and Planetary Science, 1(1), 26.

620 De Vivo, B., Lima, A., and Webster, J.D. (2005) Volatiles in Magmatic-Volcanic Systems.
621 Elements, 1(1), 19-24.

622 Deng, J., Liu, X., Wang, Q., Dilek, Y., and Liang, Y. (2017) Isotopic characterization and

petrogenetic modeling of Early Cretaceous mafic diking—Lithospheric extension in the North China craton, eastern Asia. GSA Bulletin, 129(11-12), 1379-1407.

Deng, J., Wang, Q., Santosh, M., Liu, X., Liang, Y., Yang, L., Zhao, R., and Yang, L. (2020) Remobilization of metasomatized mantle lithosphere: a new model for the Jiaodong gold province, eastern China. Mineralium Deposita, 55(2), 257-274.

Dixon, J.E., Leist, L., Langmuir, C., and Schilling, J.-G. (2002) Recycled dehydrated lithosphere observed in plume-influenced mid-ocean-ridge basalt. Nature, 420(6914), 385-389.

Dongre, A., and Tappe, S. (2019) Kimberlite and carbonatite dykes within the Premier diatreme root (Cullinan Diamond Mine, South Africa): New insights to mineralogical-genetic classifications and magma CO_2 degassing. Lithos, 338-339, 155-173.

Dou, J.-Z., Zhang, H.-F., Tong, Y., Wang, F., Chen, F.-K., and Li, S.-R. (2018) Application of geothermo-barometers to Mesozoic granitoids in the Jiaodong Peninsula, eastern China: Criteria for selecting methods of pressure estimation and implications for crustal exhumation. Journal of Asian Earth Sciences, 160, 271-286.

Ernst, W., Tsujimori, T., Zhang, R., and Liou, J. (2007) Permo-Triassic Collision, Subduction-Zone Metamorphism, and Tectonic Exhumation Along the East Asian Continental Margin. Annual Review of Earth and Planetary Sciences, 35, 73-110.

Feisel, Y., Castro, J.M., Helo, C., and Dingwell, D.B. (2022) The effect of halogens (F, Cl) on the near-liquidus crystallinity of a hydrous trachyte melt. American Mineralogist, 107(6), 1007-1017.

Filiberto, J., and Treiman, A.H. (2009a) The effect of chlorine on the liquidus of basalt: First results and implications for basalt genesis on Mars and Earth. Chemical Geology, 263(1), 60-68.

-. (2009b) Martian magmas contained abundant chlorine, but little water. Geology, 37(12), 1087-1090.

Frezzotti, M.L., and Ferrando, S. (2015) The chemical behavior of fluids released during deep subduction based on fluid inclusions. American Mineralogist, 100(2-3), 352-377.

Frezzotti, M.L., and Ferrando, S. (2018) The Role of Halogens in the Lithospheric Mantle. In D.E. Harlov, and L. Aranovich, Eds. The Role of Halogens in Terrestrial and Extraterrestrial Geochemical Processes: Surface, Crust, and Mantle, p. 805-845. Springer International Publishing.

Gaffney, A.M., Blichert-Toft, J., Nelson, B.K., Bizzarro, M., Rosing, M., and Albarède, F. (2007) Constraints on source-forming processes of West Greenland kimberlites inferred from Hf–Nd isotope systematics. Geochimica et Cosmochimica Acta, 71(11), 2820-2836.

Gao, S., Luo, T.C., Zhang, B.R., Zhang, H.F., Han, Y.W., Zhao, Z.D., and Hu, Y.K. (1998) Chemical composition of the continental crust as revealed by studies in East China. Geochimica Et Cosmochimica Acta, 62(11), 1959-1975.

Gao, S., Rudnick, R.L., Xu, W.-L., Yuan, H.-L., Liu, Y.-S., Walker, R.J., Puchtel, I.S., Liu, X., Huang, H., Wang, X.-R., and Yang, J. (2008) Recycling deep cratonic lithosphere and generation of intraplate magmatism in the North China Craton. Earth and Planetary Science Letters, 270(1), 41-53.

Guo, F., Fan, W.M., Wang, Y.J., and Zhang, M. (2004) Origin of early Cretaceous calc-alkaline lamprophyres from the Sulu orogen in eastern China: implications for enrichment processes beneath continental collisional belt. Lithos, 78(3), 291-305.

Hanley, J.J., and Koga, K.T. (2018) Halogens in Terrestrial and Cosmic Geochemical Systems: Abundances, Geochemical Behaviors, and Analytical Methods. In D.E. Harlov, and L. Aranovich, Eds. The Role of Halogens in Terrestrial and Extraterrestrial Geochemical Processes: Surface, Crust, and Mantle, p. 21-121. Springer International Publishing.

Harford, C.L. (2003) Degassing at the Soufriere Hills Volcano, Montserrat, Recorded in Matrix Glass Compositions. Journal of Petrology, 44(8), 1503-1523.

He, T., Hu, Z., Zhang, W., Chen, H., Liu, Y., Wang, Z., and Hu, S. (2019) Determination of Cl, Br, and I in Geological Materials by Sector Field Inductively Coupled Plasma Mass Spectrometry. Anal Chem, 91(13), 8109-8114.

Hecker, J.G., Marks, M.A.W., Wenzel, T., and Markl, G. (2020) Halogens in amphibole and mica from mantle xenoliths: Implications for the halogen distribution and halogen budget of the metasomatized continental lithosphere. American Mineralogist, 105(6), 781-794.

687 Hilton, D.R., Fischer, T.P., and Marty, B. (2002) Noble Gases and Volatile Recycling at
688 Subduction Zones. Reviews in Mineralogy and Geochemistry, 47(1), 319-370.

689 Hoare, B.C., Tomlinson, E.L., Barnes, J.D., Tappe, S., Marks, M.A.W., Epp, T., Caulfield,
690 J., and Riegler, T. (2021) Tracking halogen recycling and volatile loss in
691 kimberlite magmatism from Greenland: Evidence from combined F-Cl-Br and
692 δ37Cl systematics. Lithos, 105976, 384-385.

693 Ito, E., Harris, D.M., and Anderson, A.T. (1983) Alteration of Oceanic-Crust and
694 Geologic Cycling of Chlorine and Water. Geochimica Et Cosmochimica Acta,
695 47(9), 1613-1624.

696 John, T., Layne, G.D., Haase, K.M., and Barnes, J.D. (2010) Chlorine isotope evidence
697 for crustal recycling into the Earth's mantle. Earth and Planetary Science Letters,
698 298(1-2), 175-182.

699 Johnson, L.H., Burgess, R., Turner, G., and Harris, J.W. (2000) Noble gas and halogen
700 geochemistry of mantle fluids: Comparison of African and Canadian diamonds.
701 Geochimica Et Cosmochimica Acta, 64(4), 717-732.

702 Kawamoto, T., Yoshikawa, M., Kumagai, Y., Mirabueno, M.H.T., Okuno, M., and
703 Kobayashi, T. (2013) Mantle wedge infiltrated with saline fluids from dehydration
704 and decarbonation of subducting slab. Proceedings of the National Academy of
705 Sciences, 110(24), 9663-9668.

706 Kendrick, M., D'Andres, J., Holden, P., and Ireland, T. (2018) Halogens (F, Cl, Br, I) in
707 Thirteen USGS, GSJ and NIST International Rock and Glass Reference Materials.
708 Geostandards and Geoanalytical Research, 42.

709 Kendrick, M.A., Arculus, R.J., Danyushevsky, L.V., Kamenetsky, V.S., Woodhead, J.D.,
710 and Honda, M. (2014a) Subduction-related halogens (Cl, Br and I) and H_2O in
711 magmatic glasses from Southwest Pacific Backarc Basins. Earth and Planetary
712 Science Letters, 400, 165-176.

713 Kendrick, M.A., Danyushevsky, L.V., Falloon, T.J., Woodhead, J.D., Arculus, R.J., and
714 Ireland, T. (2020) SW Pacific arc and backarc lavas and the role of slab-bend
715 serpentinites in the global halogen cycle. Earth and Planetary Science Letters, 530,
716 1-12.

717 Kendrick, M.A., Hémond, C., Kamenetsky, V.S., Danyushevsky, L., Devey, C.W.,
718 Rodemann, T., Jackson, M.G., and Perfit, M.R. (2017) Seawater cycled

719 throughout Earth's mantle in partially serpentinized lithosphere. Nature
720 Geoscience, 10(3), 222-228.

721 Kendrick, M.A., Honda, M., Pettke, T., Scambelluri, M., Phillips, D., and Giuliani, A.
722 (2013) Subduction zone fluxes of halogens and noble gases in seafloor and
723 forearc serpentinites. Earth and Planetary Science Letters, 365, 86-96.

724 Kendrick, M.A., Jackson, M.G., Kent, A.J.R., Hauri, E.H., Wallace, P.J., and Woodhead, J.
725 (2014b) Contrasting behaviours of CO_2, S, H_2O and halogens (F, Cl, Br, and I) in
726 enriched-mantle melts from Pitcairn and Society seamounts. Chemical Geology,
727 370(7), 69-81.

728 Kendrick, M.A., Scambelluri, M., Honda, M., and Phillips, D. (2011) High abundances of
729 noble gas and chlorine delivered to the mantle by serpentinite subduction. Nature
730 Geoscience, 4(11), 807-812.

731 Kent, A., Peate, D., Newman, S., Stolper, E., and Pearce, J. (2002) Chlorine in submarine
732 glasses from the Lau Basin: Seawater contamination and constraints on the
733 composition of slab-derived fluids. Earth and Planetary Science Letters, 202(2),
734 361-377.

735 Kobayashi, M., Sumino, H., Burgess, R., Nakai, S.i., Iizuka, T., Nagao, J., Kagi, H.,
736 Nakamura, M., Takahashi, E., Kogiso, T., and Ballentine, C.J. (2019) Halogen
737 heterogeneity in the lithosphere and evolution of mantle halogen abundances
738 inferred from intraplate mantle xenoliths. Geochemistry, Geophysics, Geosystems,
739 20(2), 952-973.

740 Kobayashi, M., Sumino, H., Nagao, K., Ishimaru, S., Arai, S., Yoshikawa, M., Kawamoto,
741 T., Kumagai, Y., Kobayashi, T., Burgess, R., and Ballentine, C.J. (2017)
742 Slab-derived halogens and noble gases illuminate closed system processes
743 controlling volatile element transport into the mantle wedge. Earth and Planetary
744 Science Letters, 457(10), 106-116.

745 Kusky, T., Li, J., and Santosh, M. (2007) The Paleoproterozoic North Hebei Orogen:
746 North China craton's collisional suture with the Columbia supercontinent.
747 Gondwana Research, 12(1-2), 4-28.

748 Leake, and Elgey, B. (1997) Nomenclature of amphiboles; Report of the Subcommittee
749 on Amphiboles of the International Mineralogical Association, Commission on
750 New Minerals and Mineral Names. Springer Berlin Heidelberg, 82(9-10),
751 1019-1037.

752 Lesne, P., Kohn, S.C., Blundy, J., Witham, F., Botcharnikov, R.E., and Behrens, H. (2011)
753 Experimental Simulation of Closed-System Degassing in the System Basalt–
754 H_2O–CO_2–S–Cl. Journal of Petrology, 52(9), 1737-1762.

755 Li, Q.-L., Wu, F.-Y., Li, X.-H., Qiu, Z.-L., Liu, Y., Yang, Y.-H., and Tang, G.-Q. (2011)
756 Precisely dating Paleozoic kimberlites in the North China Craton and Hf isotopic
757 constraints on the evolution of the subcontinental lithospheric mantle. Lithos,
758 126(1), 127-134.

759 Liang, Y., Deng, J., Liu, X., Wang, Q., Ma, Y., Gao, T., and Zhao, L. (2019) Water
760 contents of early cretaceous mafic dikes in the Jiaodong Peninsula, Eastern North
761 China Craton: Insights into an enriched lithospheric mantle source metasomatized
762 by Paleo–Pacific Plate subduction–related fluids. The Journal of Geology, 127(3),
763 343-362.

764 Liang, Y., Deng, J., Liu, X., Wang, Q., Qin, C., Li, Y., Yang, Y., Zhou, M., and Jiang, J.
765 (2018) Major and trace element, and Sr isotope compositions of clinopyroxene
766 phenocrysts in mafic dykes on Jiaodong Peninsula, southeastern North China
767 Craton: Insights into magma mixing and source metasomatism. Lithos, 302,
768 480-495.

769 Lin, W., and Wei, W. (2018) Late Mesozoic extensional tectonics in the North China
770 Craton and its adjacent regions: a review and synthesis. International Geology
771 Review, 62(7-8), 811-839.

772 Liu, J., Cai, R., Pearson, D.G., and Scott, J.M. (2019) Thinning and destruction of the
773 lithospheric mantle root beneath the North China Craton: A review. Earth-Science
774 Reviews, 196, 102873.

775 Longpré, M.-A., Stix, J., Klügel, A., and Shimizu, N. (2017) Mantle to surface degassing
776 of carbon- and sulphur-rich alkaline magma at El Hierro, Canary Islands. Earth
777 and Planetary Science Letters, 460, 268-280.

778 Lowenstern, J.B., Bleick, H., Vazquez, J.A., Castro, J.M., and Larson, P.B. (2012)
779 Degassing of Cl, F, Li, and Be during extrusion and crystallization of the rhyolite
780 dome at Volcán Chaitén, Chile during 2008 and 2009. Bulletin of Volcanology,
781 74(10), 2303-2319.

782 Ma, L., Jiang, S.-Y., Hofmann, A.W., Dai, B.-Z., Hou, M.-L., Zhao, K.-D., Chen, L.-H.,
783 Li, J.-W., and Jiang, Y.-H. (2014a) Lithospheric and asthenospheric sources of
784 lamprophyres in the Jiaodong Peninsula: A consequence of rapid lithospheric

785 thinning beneath the North China Craton? Geochimica et Cosmochimica Acta,
786 124, 250-271.

787 Ma, L., Jiang, S.-Y., Hou, M.-L., Dai, B.-Z., Jiang, Y.-H., Yang, T., Zhao, K.-D., Pu, W.,
788 Zhu, Z.-Y., and Xu, B. (2014b) Geochemistry of Early Cretaceous calc-alkaline
789 lamprophyres in the Jiaodong Peninsula: Implication for lithospheric evolution of
790 the eastern North China Craton. Gondwana Research, 25(2), 859-872.

791 Manning, C.E., and Frezzotti, M.L. (2020) Subduction-Zone Fluids. Elements, 16(6),
792 395-400.

793 Maria, A.H., and Luhr, J.F. (2008) Lamprophyres, Basanites, and Basalts of the Western
794 Mexican Volcanic Belt: Volatile Contents and a Vein–Wallrock Melting
795 Relationship. Journal of Petrology, 49(12), 2123-2156.

796 Mcdonough, W.F., and Sun, S.S. (1995) The composition of the Earth. Chemical Geology,
797 120(3-4), 223-253.

798 Métrich, N., and Wallace, P.J. (2008) Volatile Abundances in Basaltic Magmas and Their
799 Degassing Paths Tracked by Melt Inclusions. Reviews in Mineralogy and
800 Geochemistry, 69(1), 363-402.

801 Moussallam, Y., Morizet, Y., Massuyeau, M., Laumonier, M., and Gaillard, F. (2015) CO_2
802 solubility in kimberlite melts. Chemical Geology, 418, 198-205.

803 Pagé, L., and Hattori, K. (2019) Abyssal serpentinites: Transporting halogens from
804 Earth's surface to the deep mantle. Minerals, 9(1), 61.

805 Pagé, L., Hattori, K., de Hoog, J.C.M., and Okay, A.I. (2016) Halogen (F, Cl, Br, I)
806 behaviour in subducting slabs: A study of lawsonite blueschists in western Turkey.
807 Earth and Planetary Science Letters, 442, 133-142.

808 Park, J.-W., Campbell, I.H., Kim, J., and Moon, J.-W. (2015) The Role of Late Sulfide
809 Saturation in the Formation of a Cu- and Au-rich Magma: Insights from the
810 Platinum Group Element Geochemistry of Niuatahi–Motutahi Lavas, Tonga Rear
811 Arc. Journal of Petrology, 56(1), 59-81.

812 Pokrovski, G., Borisova, A., and Bychkov, A. (2013) Speciation and Transport of Metals
813 and Metalloids in Geological Vapors, 76, 165-218.

814 Putirka, K.D. (2008) Thermometers and Barometers for Volcanic Systems. Reviews in
815 Mineralogy and Geochemistry, 69(1), 61-120.

816 Pyle, D.M., and Mather, T.A. (2009) Halogens in igneous processes and their fluxes to
817 the atmosphere and oceans from volcanic activity: A review. Chemical Geology,
818 263(1-4), 110-121.

819 Ridolfi, F., and Renzulli, A. (2012) Calcic amphiboles in calc-alkaline and alkaline
820 magmas: thermobarometric and chemometric empirical equations valid up to
821 1,130°C and 2.2 GPa. Contributions to Mineralogy and Petrology, 163(5),
822 877-895.

823 Roberge, J., Delgado-Granados, H., Wallace, P., and Kent, A. (2007) Pre-eruptive volatile
824 contents of mafic magma at Popocatépetl Volcano, Mexico, from olivine hosted
825 melt Inclusions. AGU Fall Meeting Abstracts.

826 Rock, N.M.S. (1991) Nature, Origin and Evolution of Lamprophyre Melts. In N.M.S.
827 Rock, Ed. Lamprophyres, p. 125-149. Springer US, Boston, MA.

828 Rock, N.M.S. (1987) The nature and origin of lamprophyres: an overview. Geological
829 Society, London, Special Publications, 30(1), 191-226.

830 Rock, N.M.S., and Groves, D.I. (1988) Do lamprophyres carry gold as well as diamonds?
831 Nature, 332(6161), 253-255.

832 Rudnick, R.L., and Gao, S. (2003) 3.01 - Composition of the Continental Crust. In H.D.
833 Holland, and K.K. Turekian, Eds. Treatise on Geochemistry, p. 1-64. Pergamon,
834 Oxford.

835 Ruscitto, D., Wallace, P., Cooper, L., and Plank, T. (2012) Global variations in H_2O/Ce: 2.
836 Relationships to arc magma geochemistry and volatile fluxes. Geochemistry,
837 Geophysics, Geosystems, 13, 3025.

838 Russell, J.K., Porritt, L.A., Lavallee, Y., and Dingwell, D.B. (2012) Kimberlite ascent by
839 assimilation-fuelled buoyancy. Nature, 481(7381), 352-6.

840 Russell, J.K., Sparks, R.S.J., and Kavanagh, J.L. (2019) Kimberlite Volcanology:
841 Transport, Ascent, and Eruption. Elements, 15(6), 405-410.

842 Rustioni, G., Audetat, A., and Keppler, H. (2021) The composition of subduction zone
843 fluids and the origin of the trace element enrichment in arc magmas.
844 Contributions to Mineralogy and Petrology, 176(7),1-19.

845 Saal, A., Hauri, E., Langmuir, C., and Perfit, M. (2002) Vapor Undersaturation in
846 Primitive MORBs and the Volatile Content of the Earth's Upper Mantle. Nature,

847 66(15A), 451-455.

848 Schilling, J.G., Unni, C.K., and Bender, M.L. (1978) Origin of chlorine and bromine in
849 the oceans. Nature, 273(5664), 631-636.

850 Sekimoto, S., and Ebihara, M. (2017) Accurate Determination of Chlorine, Bromine and
851 Iodine in U.S. Geological Survey Geochemical Reference Materials by
852 Radiochemical Neutron Activation Analysis. Geostandards and Geoanalytical
853 Research, 41(2), 213-219.

854 Shagalov, E., Holodnov, V., Sustavov, S., and Kiseleva, D. (2021) Cl-rich amphiboles and
855 micas in rocks of the Middle Riphean Kusa-Kopan complex of mafic layered
856 intrusions (southern Urals, Russia). Mineralogy and Petrology, 115, 1-19.

857 Shen, L., Hu, R., Shan, G., Feng, C., Yu, B., Feng, G., Qi, Y., Tao, W., and Coulson, I.M.
858 (2009) Petrogenesis of Late Mesozoic mafic dykes in the Jiaodong Peninsula,
859 eastern North China Craton and implications for the foundering of lower crust.
860 Lithos, 113(3-4), 621-639.

861 Spilliaert, N., Métrich, N., and Allard, P. (2006) S–Cl–F degassing pattern of water-rich
862 alkali basalt: Modelling and relationship with eruption styles on Mount Etna
863 volcano. Earth and Planetary Science Letters, 248(3), 772-786.

864 Stroncik, N.A., and Haase, K.M. (2004) Chlorine in oceanic intraplate basalts:
865 Constraints on mantle sources and recycling processes. Geology, 32(11), 945.

866 Sumino, H., Burgess, R., Mizukami, T., Wallis, S.R., Holland, G., and Ballentine, C.J.
867 (2010) Seawater-derived noble gases and halogens preserved in exhumed mantle
868 wedge peridotite. Earth and Planetary Science Letters, 294(1-2), 163-172.

869 Taylor, W.R., Rock, N.M.S., Groves, D.I., Perring, C.S., and Golding, S.D. (1994)
870 Geochemistry of Archean shoshonitic lamprophyres from the Yilgarn Block,
871 Western Australia: Au abundance and association with gold mineralization.
872 Applied Geochemistry, 9(2), 197-222.

873 Teiber, H., Marks, M.A.W., Wenzel, T., Siebel, W., Altherr, R., and Markl, G. (2014) The
874 distribution of halogens (F, Cl, Br) in granitoid rocks. Chemical Geology, 374-375,
875 92-109.

876 Thomas, R.W., and Wood, B.J. (2021) The chemical behaviour of chlorine in silicate
877 melts. Geochimica et Cosmochimica Acta, 294, 28-42.

878 Tomlinson, E.L., Jones, A.P., and Harris, J.W. (2006) Co-existing fluid and silicate
879 inclusions in mantle diamond. Earth and Planetary Science Letters, 250(3),
880 581-595.

881 Toyama, C., Muramatsu, Y., Yamamoto, J., Nakai, S., rsquo, Ichi, and Kaneoka, I. (2012)
882 Sr and Nd isotope ratios and trace element concentrations in kimberlites from
883 Shandong and Liaoning (China) and the Kimberley area (South Africa).
884 GEOCHEMICAL JOURNAL, 46(1), 45-59.

885 Toyama, C., Sumino, H., Okabe, N., Ishikawa, A., Yamamoto, J., Kaneoka, I., and
886 Muramatsu, Y. (2021) Halogen heterogeneity in the subcontinental lithospheric
887 mantle revealed by I/Br ratios in kimberlites and their mantle xenoliths from
888 South Africa, Greenland, China, Siberia, Canada, and Brazil. American
889 Mineralogist, 106(12), 1890-1899.

890 Tripathi, P., Pandey, O.P., Srivastava, J.P., Sachan, H.K., Subbarao, D.V., Satyanabueanan,
891 M., Krishna, A.K., Vedanti, N., Reddy, G.K., Rasheed, K., Dwivedi, S.K., and
892 Parthasarathy, G. (2021) Amphibolite-granulite facies mid-crustal basement in
893 Deccan Large Igneous Province and its implication on Precambrian crustal
894 evolution: evidence from Killari borehole studies. International Journal of Earth
895 Sciences, 110(8), 2661-2683.

896 Ubide, T., Larrea, P., Becerril, L., and Galé, C. (2022) Volcanic plumbing filters on
897 ocean-island basalt geochemistry. Geology, 50(1), 26-31.

898 Unni, C., and Schilling, J.-G. (1978) Cl and Br degassing by volcanism along the
899 Reykjanes Ridge and Iceland. Nature, 272(5648), 19-23.

900 von Glasow, R., Bobrowski, N., and Kern, C. (2009) The effects of volcanic eruptions on
901 atmospheric chemistry. Chemical Geology, 263(1), 131-142.

902 Waelkens, C.M., Stix, J., Monteleone, B., and Burckel, P. (2021) Efficient release of
903 bromine by super-eruptions. Geology, 49(12), 1416-1420.

904 Wallace, P.J. (2005) Volatiles in subduction zone magmas: concentrations and fluxes
905 based on melt inclusion and volcanic gas data. Journal of Volcanology and
906 Geothermal Research, 140(1), 217-240.

907 Wang, L.-X., Marks, M.A.W., Keller, J., and Markl, G. (2014) Halogen variations in
908 alkaline rocks from the Upper Rhine Graben (SW Germany): Insights into F, Cl
909 and Br behavior during magmatic processes. Chemical Geology, 380(13),

133-144.

Wang, Q., Makishima, A., and Nakamura, E. (2010) Determination of Fluorine and Chlorine by Pyrohydrolysis and Ion Chromatography: Comparison with Alkaline Fusion Digestion and Ion Chromatography. Geostandards and Geoanalytical Research, 34, 175-183.

Wang, X., Wang, Z., Cheng, H., Zong, K., Wang, C.Y., Ma, L., Cai, Y.-C., Foley, S., and Hu, Z. (2022) Gold endowment of the metasomatized lithospheric mantle for giant gold deposits: Insights from lamprophyre dykes. Geochimica et Cosmochimica Acta, 316, 21-40.

Wang, X., Wang, Z.C., Cheng, H., Foley, S., Xiong, L., and Hu, Z.C. (2020) Early cretaceous lamprophyre dyke swarms in Jiaodong Peninsula, eastern North China Craton, and implications for mantle metasomatism related to subduction. Lithos, 368, 105593.

Webster, J., Kinzler, R., and Mathez, E.A. (1999) Chloride and water solubility in basalt and andesite melts and implications for magma degassing. Geochimica et Cosmochimica Acta, 63(5), 729-738.

Webster, J.D. (2004) The exsolution of magmatic hydrosaline chloride liquids. Chemical Geology, 210(1-4), 33-48.

Webster, J.D., Baker, D.R., and Aiuppa, A. (2018) Halogens in Mafic and Intermediate-Silica Content Magmas. In D.E. Harlov, and L. Aranovich, Eds. Isotopic characterization and petrogeneti Geochemical Processes: Surface, Crust, and Mantle, p. 307-430. Springer International Publishing.

Webster, J.D., and De Vivo, B. (2002) Experimental and modeled solubilities of chlorine in aluminosilicate melts, consequences of magma evolution, and implications for exsolution of hydrous chloride melt at Mt. Somma-Vesuvius. American Mineralogist, 87(8-9), 1046-1061.

Weiss, Y., McNeill, J., Pearson, D.G., Nowell, G.M., and Ottley, C.J. (2015) Highly saline fluids from a subducting slab as the source for fluid-rich diamonds. Nature, 524(7565), 339-342.

Windley, B.F., Maruyama, S., and Xiao, W.J. (2010) Delamination/thinning of sub-continental lithospheric mantle under Eastern China: The role of water and multiple subduction. American Journal of Science, 310(10), 1250–1293.

Workman, R.K., Hauri, E., Hart, S.R., Wang, J., and Blusztajn, J. (2006) Volatile and trace elements in basaltic glasses from Samoa: Implications for water distribution in the mantle. Earth and Planetary Science Letters, 241(3), 932-951.

Wu, F.Y., Yang, J.H., Xu, Y.G., Wilde, S.A., and Walker, R.J. (2019) Destruction of the North China Craton in the Mesozoic. Annual Review of Earth and Planetary Sciences, Vol 47, 47(1), 173-195.

Xia, Q.-K., Liu, J., Kovács, I., Hao, Y.-T., Li, P., Yang, X.-Z., Chen, H., and Sheng, Y.-M. (2019) Water in the upper mantle and deep crust of eastern China: concentration, distribution and implications. National Science Review, 6(1), 125-144.

Xia, Q.-K., Liu, J., Liu, S.-C., Kovács, I., Feng, M., and Dang, L. (2013) High water content in Mesozoic primitive basalts of the North China Craton and implications on the destruction of cratonic mantle lithosphere. Earth and Planetary Science Letters, 361, 85-97.

Zajacz, Z., Halter, W.E., Pettke, T., and Guillong, M. (2008) Determination of fluid/melt partition coefficients by LA-ICPMS analysis of co-existing fluid and silicate melt inclusions: Controls on element partitioning. Geochimica et Cosmochimica Acta, 72(8), 2169-2197.

Zajacz, Z., Seo, J.H., Candela, P.A., Piccoli, P.M., Heinrich, C.A., and Guillong, M. (2010) Alkali metals control the release of gold from volatile-rich magmas. Earth and Planetary Science Letters, 297(1-2), 50-56.

Zhang, C., Holtz, F., Ma, C., Wolff, P.E., and Li, X. (2012) Tracing the evolution and distribution of F and Cl in plutonic systems from volatile-bearing minerals: a case study from the Liujiawa pluton (Dabie orogen, China). Contributions to Mineralogy and Petrology, 164(5), 859-879.

Zhang, R.X., and Yang, S.Y. (2016) A Mathematical Model for Determining Carbon Coating Thickness and Its Application in Electron Probe Microanalysis. Microsc Microanal, 22(6), 1374-1380.

Zhao, G., Wilde, S.A., Cawood, P.A., and Sun, M. (2001) Archean blocks and their boundaries in the North China Craton: lithological, geochemical, structural and P–T path constraints and tectonic evolution. Precambrian Research, 107(1-2), 45-73.

Zheng, Y., Xu, Z., Zhao, Z., and Dai, L. (2018) Mesozoic mafic magmatism in North China: Implications for thinning and destruction of cratonic lithosphere. Science

974 China Earth Sciences, 61(4), 353-385.

975 Zimova, M., and Webb, S. (2006) The effect of chlorine on the viscosity of
976 Na_2O-Fe_2O_3-Al_2O_3-SiO_2 melts. American Mineralogist, 91(2-3), 344-352.

977 **Figure captions**

978 Fig. 1. Simplified geological map showing the distribution of the Early Cretaceous
979 lamprophyres, basalts, and Paleozoic kimberlites in the eastern North China Craton. (a)
980 The location of the Jiaodong Peninsula and the spatial distribution of kimberlites and
981 basalts in Shandong (Mengyin, Jining, and Feixian) and Liaoning (Wafangdian). (b) The
982 location of studied lamprophyres, modified from Deng et al. (2020) and Wang et al.
983 (2022).

984

985 Fig. 2. Field and microphotographs of lamprophyre dykes in the Jiaodong Peninsula. (a)
986 Lamprophyre dykes (130–120 Ma) intruding into the Linglong granite in an underground
987 shaft. (b) Clinopyroxene phenocrysts in lamprophyre. (c, d) Representative
988 microphotographs of fresh lamprophyres of this study. Volatile-rich minerals (amphibole
989 and biotite) occur widely. (e, f) Representative microphotographs of altered lamprophyres.
990 The phenocrysts are chloritized to variable degrees. Microphotographs were under
991 plane-polarized transmitted light. (g, h) Backscattered electron images of amphiboles in
992 fresh lamprophyres (17XS26). The circles are analysis spots for electron microprobe
993 analysis. Cpx - clinopyroxene; Pl - plagioclase; Amp - amphibole; Bt - biotite; Ap -
994 Apatite.

995

996 Fig. 3. Trace elements and Sr-Nd isotopic characteristics of lamprophyres, kimberlites,
997 and basalts. Primitive mantle-normalized trace element patterns for lamprophyres and
998 basalts are similarly arc-like. Kimberlites are enriched in incompatible elements and
999 depleted in Sr. Data for lamprophyres, kimberlites, and Feixian basalts were obtained
1000 from Wang et al. (2020), Toyama et al. (2012), and Gao et al. (2008), respectively;
1001 Primitive mantle data from Mcdonough and Sun (1995); Compositional range of MORB
1002 and OIB from Wang et al. (2020) and the references therein.
1003
1004 Fig. 4. Halogen concentrations of the lamprophyres in this study. (a, b) Bulk-rock Cl and
1005 Br concentrations versus MgO contents. (c, d) Comparison of Br, Cl, and I concentrations.
1006 Note the I concentrations are below the detection limit of 5 ng/g. Lamprophyres have
1007 relatively low halogen contents and there is no correlation among halogens and between
1008 halogens and MgO for lamprophyres. Database for comparison: MORBs and OIBs
1009 (Kendrick et al., 2017); Arc-related lavas (Kendrick et al., 2020; Park et al., 2015);
1010 Kimberlites (Gaffney et al., 2007; Hoare et al., 2021; Toyama et al., 2012; Toyama et al.,
1011 2021); Glass inclusions in olivine of lamprophyres from Mexico (Maria and Luhr, 2008).
1012
1013 Fig. 5. Comparison of fluid-mobile halogen concentrations with fluid-immobile Nb.
1014 MORBs and OIBs show good positive correlations of Cl, Br, I, and Nb, indicating their

similar incompatibility during mantle melting and fractional crystallization. The higher halogen concentrations of arc-related lavas reflect the addition of fluid-mobile Cl, Br, and I by subduction. The halogen concentrations in lamprophyres are similar to MORB at a given Nb concentration. Data for comparison are the same as in Fig. 4.

Fig. 6. Comparison of Cl and Br concentrations with K. (a, b) MORBs, OIBs, and arc lava data show good positive correlations of Cl, Br, and K, indicating their similar behavior during magmatic processes and subduction. However, the Cl and Br concentrations in lamprophyres are much lower at given K contents indicating strong depletion of Cl and Br. (c, d) Cl/K and Br/K ratios of lamprophyres are also obviously lower than those of MORBs, OIBs, and arc-related lavas.

Fig. 7. Halogens, Ba, and K relative to the fluid immobile lithophile element of similar incompatibility (Nb). The Cl/Nb and Br/Nb of the arc-related lavas show positive correlations with K/Nb and Ba/Nb, suggesting that Cl, Br, K, and Ba are added into the source regions effectively during subduction and negligible degassing during eruption. However, at given K/Nb and Ba/Nb, the ratios of Cl/Nb and Br/Nb in lamprophyres are lower than arc lavas, indicating volatile loss of Cl and Br.

Fig. 8. Halogen concentrations and Br/Cl ratios of lamprophyres with different degrees of alteration. (a) Average halogen compositions of fresh and chloritized samples. (b) Br/Cl vs MgO content, showing melt evolution is not responsible for the variable Br/Cl ratios. (c) Br/Cl vs Ba/Nb, showing elevated Br/Cl ratios are unrelated to mantle metasomatism.

Fig. 9. Synoptic diagram showing the generation, transport, and exsolution of halogen-rich fluid in ascending primitive magmas of lamprophyre from the metasomatized lithospheric mantle to the middle crust. The metasomatic portions of the lithospheric mantle are rich in halogens and other fluid-mobile elements. Crystallization of nominally-volatile-free minerals and reaction with surrounding mantle rocks induced fluid exsolution which led to significant loss of volatile halogens.

Table 1. Halogen compositions of lamprophyres from Jiaodong Peninsula.

Table 2. Chemical composition of amphiboles and clinopyroxenes in lamprophyres from Jiaodong Peninsula.

Supplementary Figure 1–2

- Fig. S1: Comparison of I concentrations with Nb and K.

-Fig. S2: The pressures and water contents of melts at the time of amphibole

1053 crystallization. The solubility curves represent the maximum concentrations of H_2O in the
1054 basaltic melts at a given pressure. Modified from (Newman and Lowenstern, 2002)
1055 Supplementary Table 1–4
1056 - Table S1: Major (wt.%), trace element (μg/g), and Sr-Nd isotopes data for the
1057 lamprophyres from Jiaodong Peninsula.
1058 - Table S2: Compositions (wt.% averages ± 1σ standard deviations) of representative
1059 fresh amphibole in lamprophyres from Jiaodong Peninsula.
1060 - Table S3: Compositions (wt.% averages ± 1σ standard deviations) of representative
1061 fresh clinopyroxene in lamprophyres from Jiaodong Peninsula.
1062 - Table S4: Trace element (μg/g) and Sr-Nd isotopes data for the kimberlites from Eastern
1063 China.

Table 1. Halogen compositions of lamprophyres from Jiaodong Peninsula

	Mg#[d]	LOI [e] wt.%	Cl µg/g	Br ng/g	I ng/g	Cl/K $\times10^{-3}$	Br/K $\times10^{-3}$	Ba/Nb	Cl/Nb	Br/Nb	Br/Cl	Cl_{recalc} [f] µg/g	Br_{recalc} [f] ng/g	I_{recalc} [f] ng/g	Cl loss %	Br loss %	I loss[g] %
17XS26 [a]	69	4.65	168 ± 2.5	362 ± 36	< 5	10	0.02	192	22	0.05	0.002	1581	4362	93	89	92	95
17QX20B [a]	72	5.62	145 ± 2.5	321 ± 36	< 5	9	0.02	404	29	0.06	0.002	1490	4109	88	90	92	94
17QX20C [a]	74	5.73	150 ± 2.5	285 ± 36	< 5	9	0.02	385	29	0.05	0.002	1453	4008	85	90	93	94
17XS06[b]	73	11.27	74 ± 3.0	322 ± 36	< 5	4	0.02	261	15	0.06	0.004	1635	4510	96	95	93	95
17XS08 [b]	67	8.38	136 ± 2.4	379 ± 35	< 5	7	0.02	170	16	0.04	0.003	1711	4719	100	92	92	95
17XS09 [b]	66	8.60	118 ± 2.5	447 ± 35	< 5	6	0.02	188	14	0.05	0.004	1745	4813	102	93	91	95
17XS11 [b]	66	8.04	111 ± 2.5	386 ± 35	< 5	8	0.02	196	13	0.04	0.003	1332	3673	78	92	89	94
17XS12 [b]	66	9.88	62 ± 3.4	495 ± 36	< 5	3	0.02	282	7	0.05	0.008	1943	5359	114	97	91	96
17XS14 [b]	69	6.10	170 ± 2.5	325 ± 36	< 5	10	0.02	153	26	0.05	0.002	1360	3750	80	88	91	94
Replicate [h]			172 ± 2.6	370 ± 38	< 5												
17XS18 [b]	71	8.28	78 ± 3.0	450 ± 36	< 5	4	0.02	281	17	0.1	0.005	1732	4778	101	95	91	95
17XS23 [b]	70	6.91	67 ± 3.3	502 ± 37	< 5	4	0.03	321	14	0.1	0.007	1399	3858	82	95	87	94
17XS25 [b]	68	9.00	81 ± 2.8	559 ± 35	< 5	5	0.03	268	18	0.1	0.007	1569	4327	92	95	87	95
17XS27 [b]	71	3.53	160 ± 2.7	411 ± 38	< 5	9	0.02	302	26	0.06	0.002	1709	4715	100	91	91	95
17XS16 [c]	69	10.67	60 ± 3.9	518 ± 36	< 5	3	0.02	328	13	0.1	0.008	1782	4914	104	97	89	95

17QX21 [c]	73	9.78	58 ± 3.5	496 ± 37	< 5	2	0.01	368	6	0.05	0.008	2907	8019	170	98	94	97
17ZY26 [c]	66	8.72	71 ± 3.1	528 ± 36	< 5	3	0.02	269	9	0.06	0.007	2493	6878	146	97	92	97
BHVO-2			99 ± 2.8	252 ± 36	42 ± 2.1												

Notes: Errors are standard deviation of repeated analyses (n = 3). The major and trace element contents and Sr-Nd isotopes have been published before (Wang et al., 2020), and see Supplementary Table S1 for details.

[a, b, c] represent fresh, slight chloritization, and intense chloritization, respectively.

[d] Mg# = 100× Mg/ (Mg + Fe) in molar fraction.

[e] LOI=loss on ignition.

[f] Halogens with recaclc subscript are estimates of the original magma composition assuming a Cl/K ratio of 0.091, a Br/K ratio of 2.5×10^{-4} and a I/K ratio of 5.3×10^{-6} (see text).

[g] The loss ratio of I is calculated based on the detection limit (5 ng/g). The calculated theoretical I concentration and the actual loss ratio should be higher.

[h] The replicate from different aliquot of sample powder (17XS14).

This is the peer-reviewed, final accepted version for American Mineralogist, published by the Mineralogical Society of America.
The published version is subject to change. Cite as Authors (Year) Title. American Mineralogist, in press.
DOI: https://doi.org/10.2138/am-2022-8693. http://www.minsocam.org/

Table 2. Chemical composition of amphiboles and clinopyroxenes in lamprophyres from Jiaodong Peninsula

Lamprophyres	Mineral	SiO_2 wt.%	TiO_2 wt.%	Al_2O_3 wt.%	FeO[a] wt.%	MgO wt.%	CaO wt.%	Na_2O wt.%	K_2O wt.%	F wt.%	Cl wt.%	Total wt.%	Mg#[b]	X_F[c]	X_{Cl}[c]	X_{OH}[c]	P[d] Mpa	T[d] ℃	H_2O_{melt}[d] wt.%	Depth[e] km
17XS26	Amp-1	42.33	3.06	11.98	12.59	13.71	11.51	1.62	1.10	0.98	0.02	98.42	66	0.44	0.00	1.54	420	924	6.27	15.9
	Amp-2	43.03	2.81	11.41	12.59	13.93	11.42	1.62	1.04	1.03	0.02	98.52	66	0.47	0.00	1.55	360	911	6.05	13.6
	Amp-3	43.06	2.42	11.33	13.34	13.59	11.29	1.62	0.99	1.07	0.02	98.05	64	0.49	0.01	1.50	340	907	6.18	12.8
	Amp-4	42.78	2.86	11.65	12.70	13.78	11.37	1.63	1.06	1.01	0.02	98.45	66	0.47	0.01	1.52	387	915	6.21	14.6
17QX20C	Cpx	51.88	0.67	3.60	5.38	15.37	22.22	0.22	0.00	—	—	99.81	84	—	—	—	278	1169	—	10.5
17XS18	Cpx	52.49	0.37	2.99	5.27	16.47	20.50	0.27	0.00	—	—	99.04	85	—	—	—	524	1214	—	19.8
17XS26	Cpx	50.68	0.71	4.44	5.62	14.95	21.23	0.29	0.00	—	—	98.88	83	—	—	—	542	1200	—	20.5
17XS27	Cpx	51.97	0.45	3.58	5.62	16.05	20.35	0.31	0.00	—	—	99.01	84	—	—	—	594	1215	—	22.4

[a] Total iron expressed as FeO.

[b] Mg# = 100×Mg / (Mg + Fe) in molar fraction.

[c] X_F, X_{Cl}, X_{OH} represent mole fractions of corresponding volatile components in amphibole formula, calculated with methods of Zhang et al. (2012).

[d] P, T, H_2O_{melt} represent the pressure, temperature conditions and water contents at the time of amphibole crystallization, calculated according to Ridolfi and Renzulli (2012) and Putirka (2008) for amphiboles and clinopyroxenes, respectively. The electron microprobe data of clinopyroxenes are from Wang et al. (2022).

[e] The average crustal density used in depth calculations is 2.7 g /cm^3.

See details for amphiboles and clinopyroxenes chemical compositions in Supplementary Table S2 and Table S3.

This is the peer-reviewed, final accepted version for American Mineralogist, published by the Mineralogical Society of America.
The published version is subject to change. Cite as Authors (Year) Title. American Mineralogist, in press.
DOI: https://doi.org/10.2138/am-2022-8693. http://www.minsocam.org/

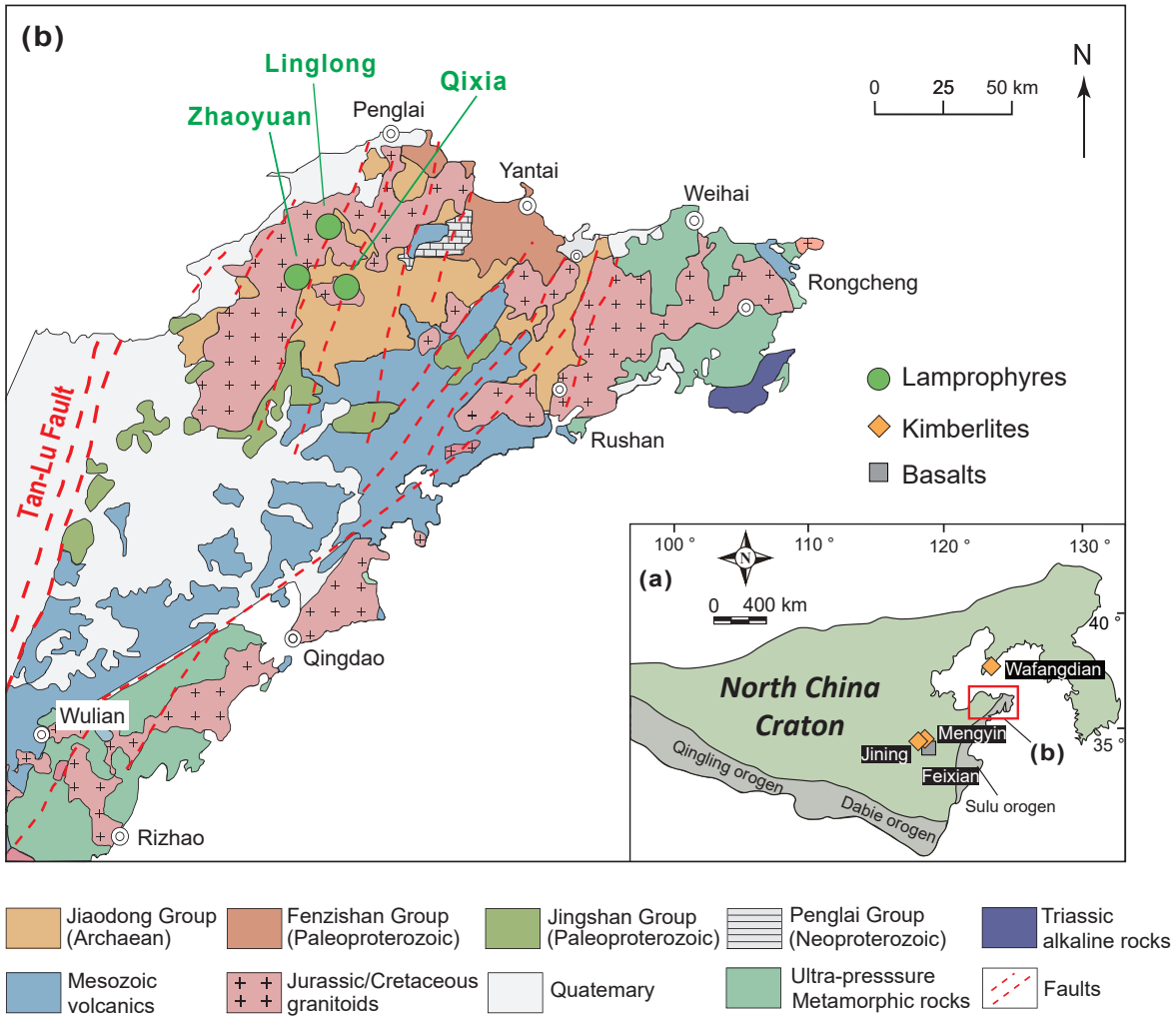

Fig. 1

This is the peer-reviewed, final accepted version for American Mineralogist, published by the Mineralogical Society of America.
The published version is subject to change. Cite as Authors (Year) Title. American Mineralogist, in press.
DOI: https://doi.org/10.2138/am-2022-8693. http://www.minsocam.org/

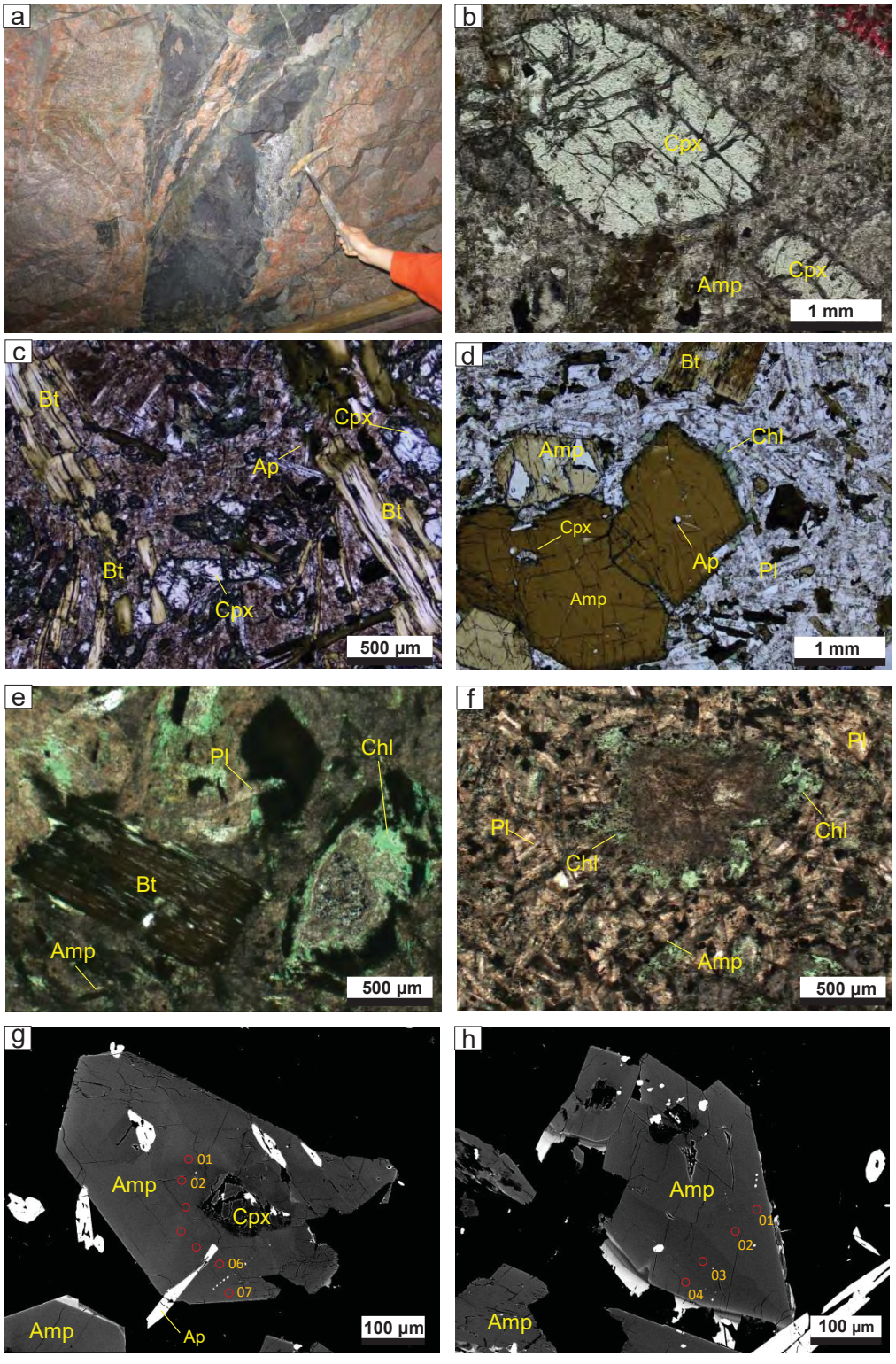

Fig. 2

This is the peer-reviewed, final accepted version for American Mineralogist, published by the Mineralogical Society of America.
The published version is subject to change. Cite as Authors (Year) Title. American Mineralogist, in press.
DOI: https://doi.org/10.2138/am-2022-8693. http://www.minsocam.org/

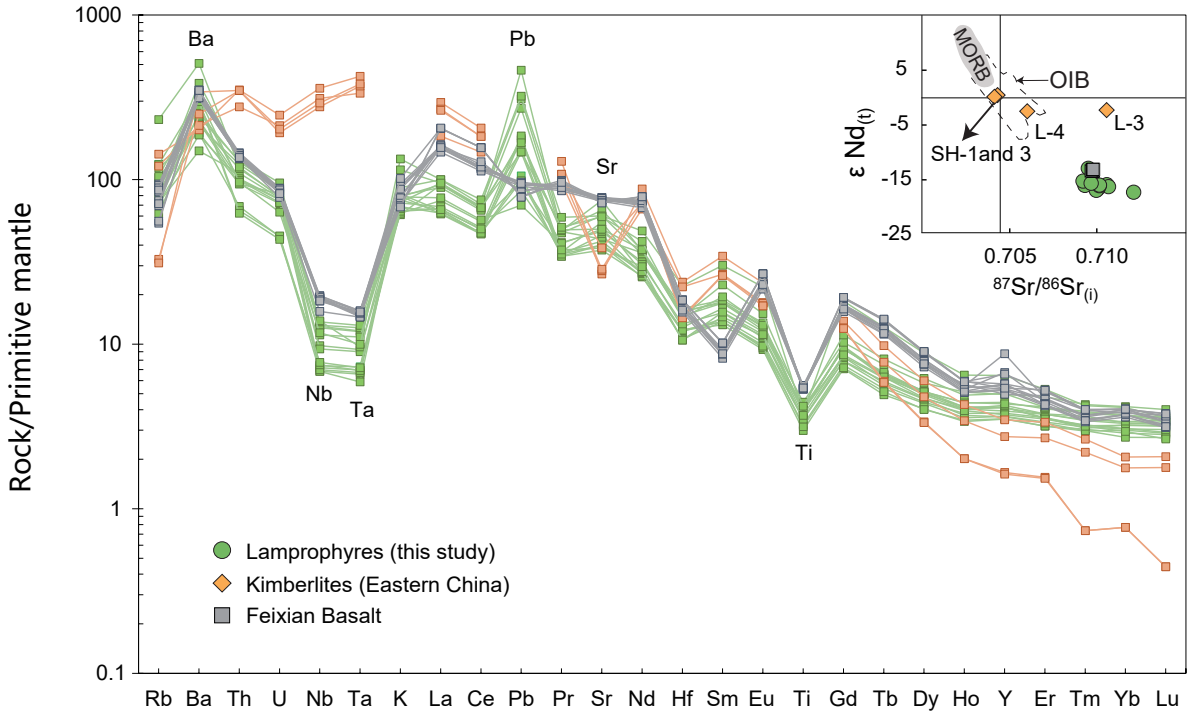

Fig. 3

This is the peer-reviewed, final accepted version for American Mineralogist, published by the Mineralogical Society of America.
The published version is subject to change. Cite as Authors (Year) Title. American Mineralogist, in press.
DOI: https://doi.org/10.2138/am-2022-8693. http://www.minsocam.org/

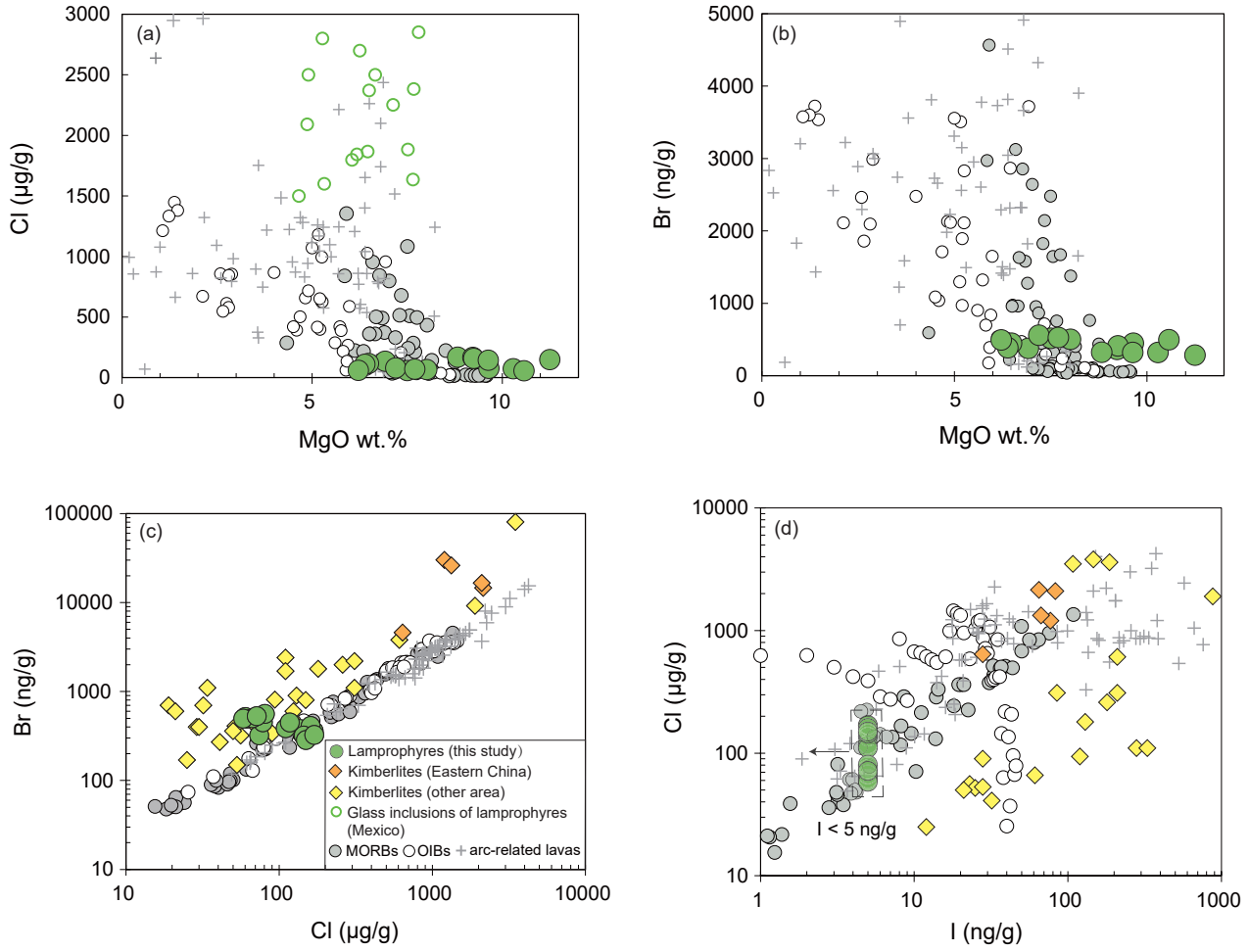

Fig. 4

This is the peer-reviewed, final accepted version for American Mineralogist, published by the Mineralogical Society of America.
The published version is subject to change. Cite as Authors (Year) Title. American Mineralogist, in press.
DOI: https://doi.org/10.2138/am-2022-8693. http://www.minsocam.org/

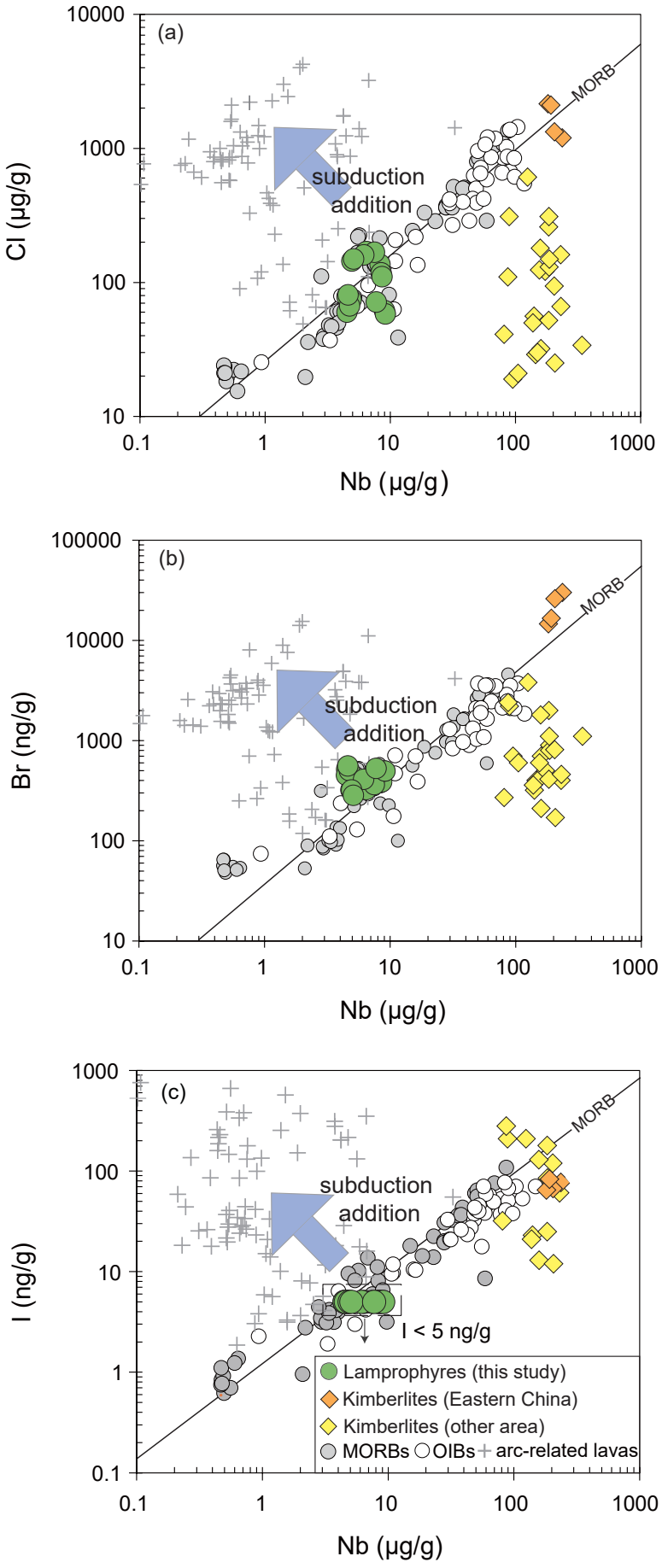

Fig. 5

This is the peer-reviewed, final accepted version for American Mineralogist, published by the Mineralogical Society of America.
The published version is subject to change. Cite as Authors (Year) Title. American Mineralogist, in press.
DOI: https://doi.org/10.2138/am-2022-8693. http://www.minsocam.org/

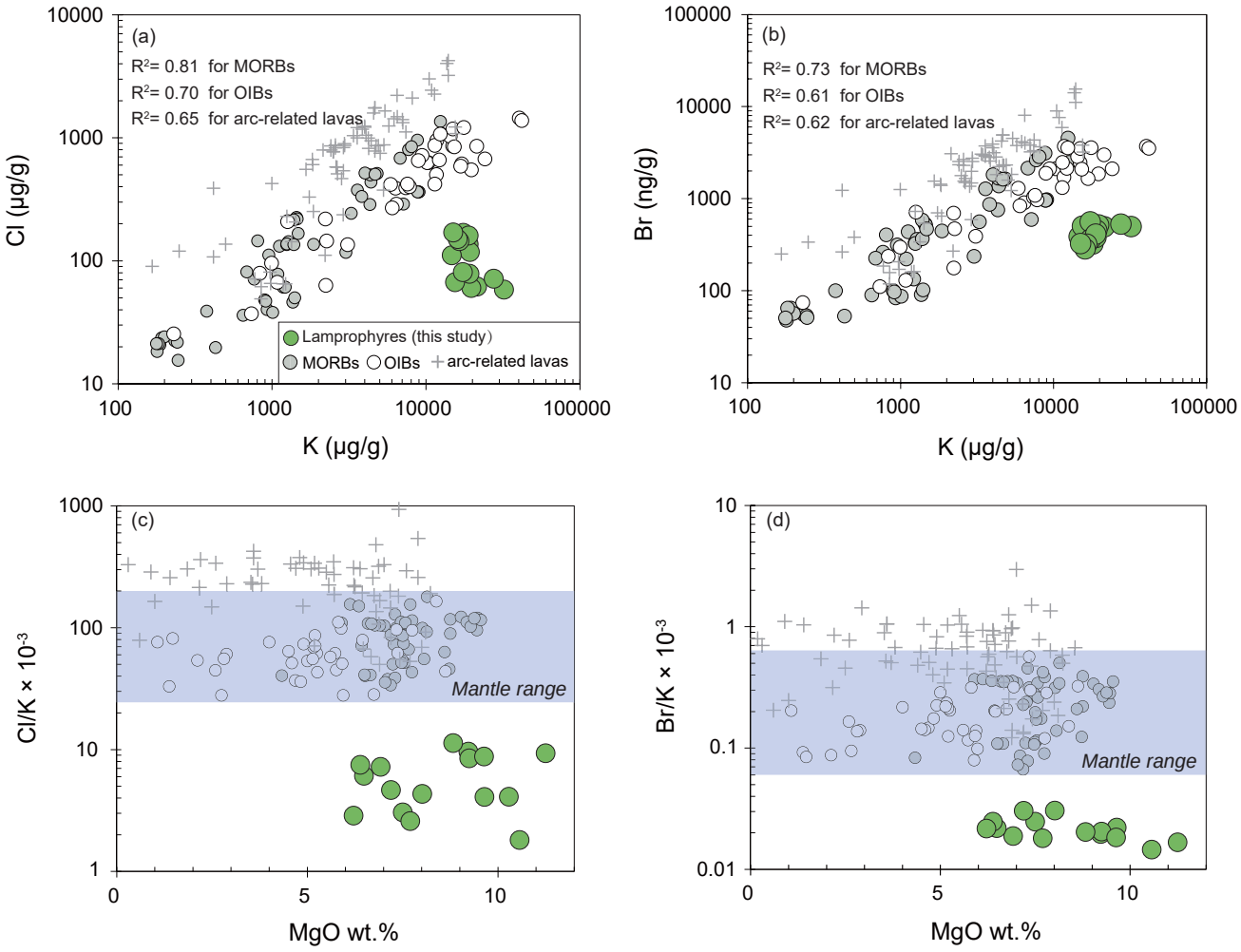

Fig. 6

This is the peer-reviewed, final accepted version for American Mineralogist, published by the Mineralogical Society of America.
The published version is subject to change. Cite as Authors (Year) Title. American Mineralogist, in press.
DOI: https://doi.org/10.2138/am-2022-8693. http://www.minsocam.org/

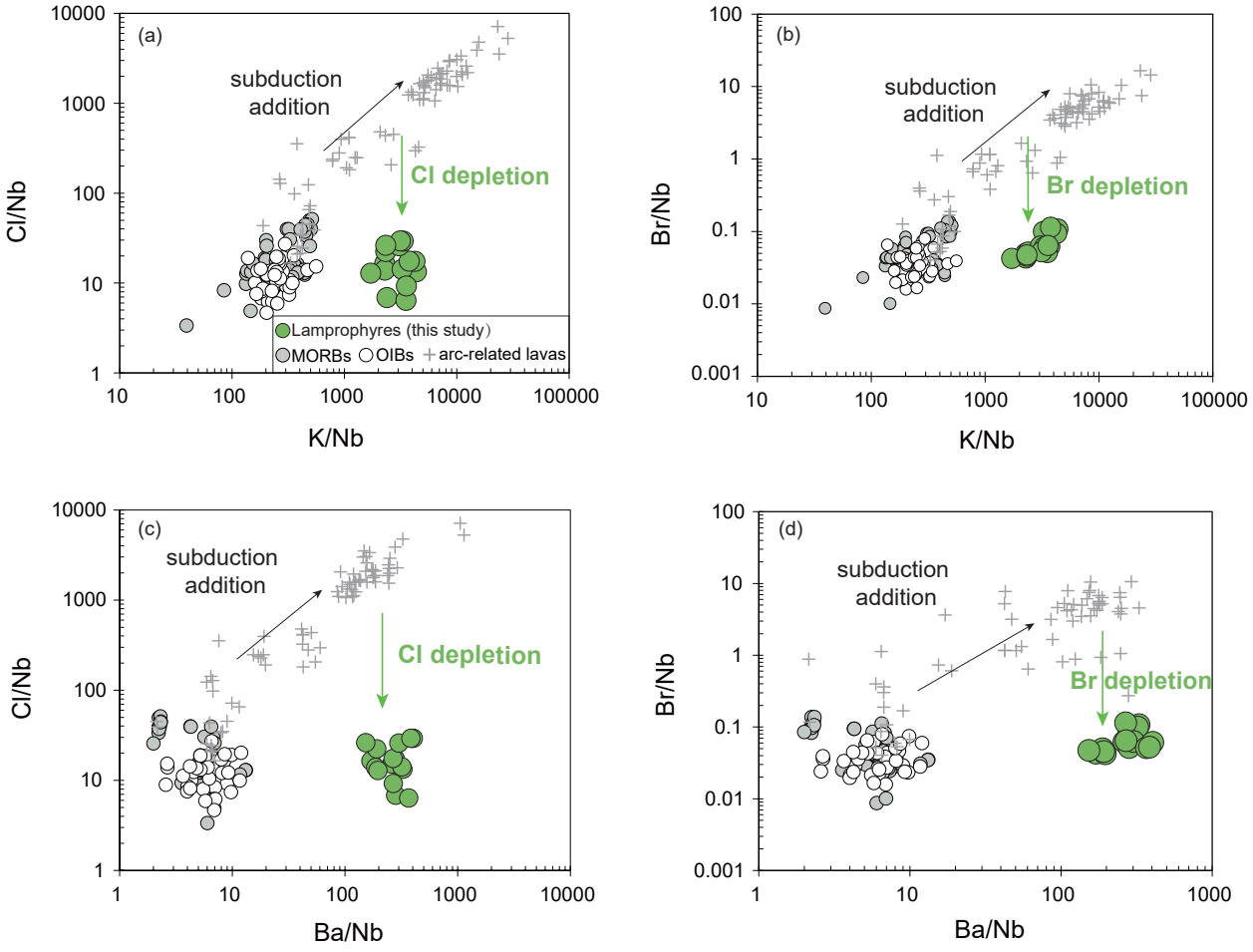

Fig. 7

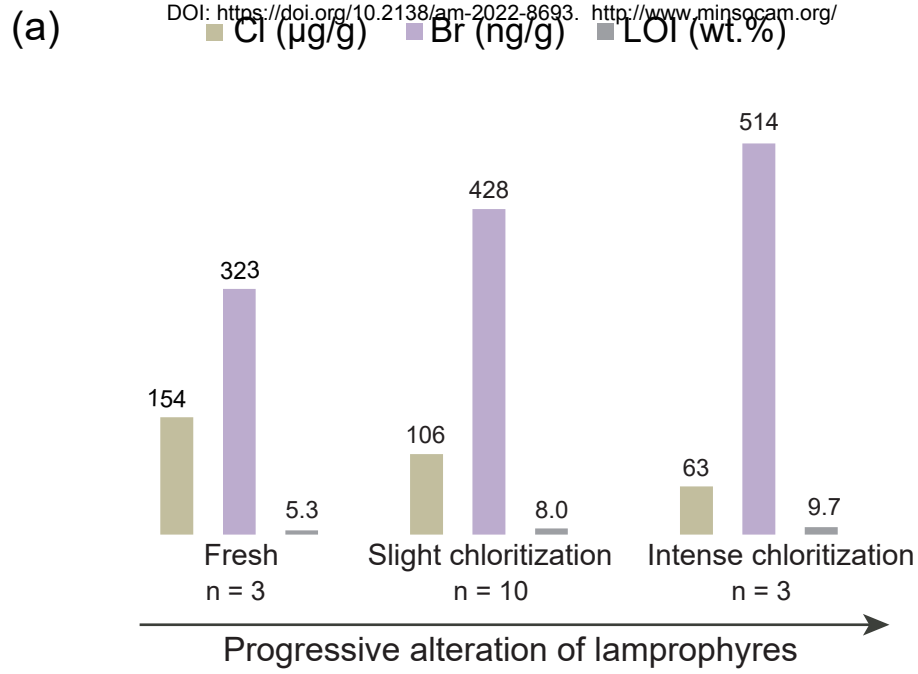

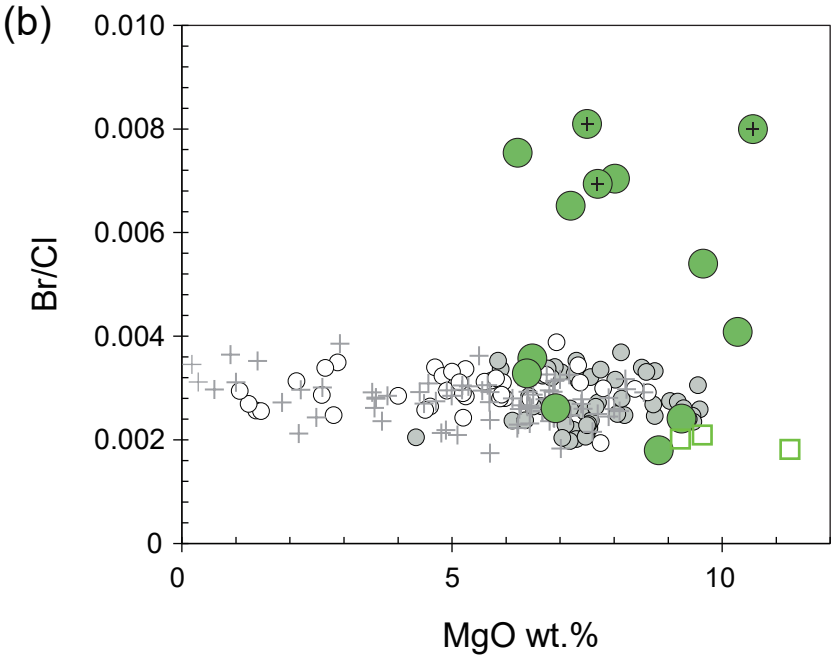

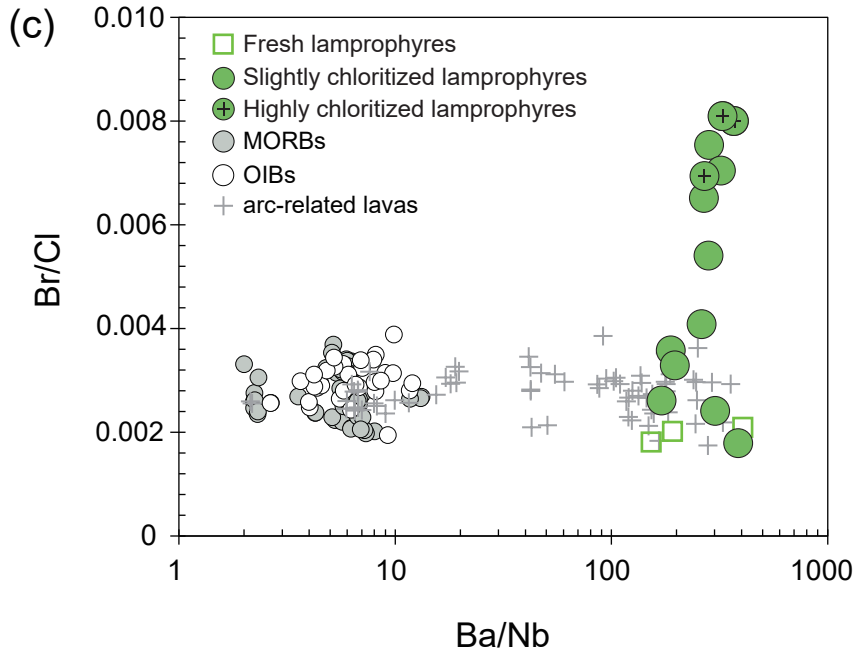

Fig. 8

This is the peer-reviewed, final accepted version for American Mineralogist, published by the Mineralogical Society of America.
The published version is subject to change. Cite as Authors (Year) Title. American Mineralogist, in press.
DOI: https://doi.org/10.2138/am-2022-8693. http://www.minsocam.org/

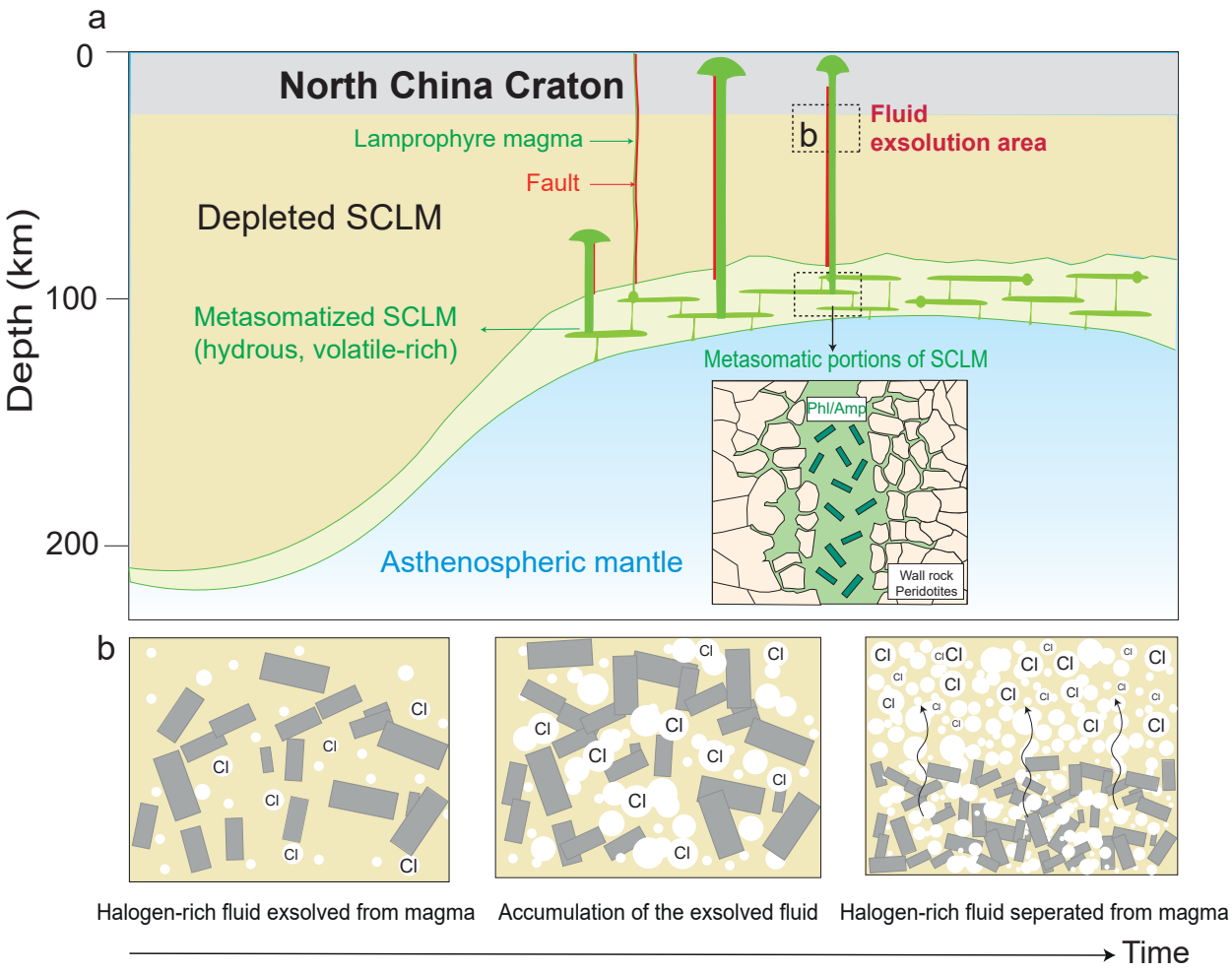

Fig. 9